P
12 mint

REPORT NO. P73-282

# DEVELOPMENT OF PORCELAIN ENAMEL PASSIVE THERMAL CONTROL COATINGS

FINAL REPORT

H. Levin
W. E. Lent
D. H. Buettner

(NASA-CR-124459) DEVELOPMENT OF PORCELAIN ENAMEL PASSIVE THERMAL CONTROL COATINGS Final Report, 1 Jul. 1972 - 20 Jul. 1973 (Hughes Aircraft Co.) ~~83~~ 80 p HC $6.25 CSCL 11D G3/18 N73-33459 Unclas 15748

SEPTEMBER 1973





(DCN1-2-50-23682)

Prepared under Contract No. NAS8-27439 by
HUGHES AIRCRAFT COMPANY
Culver City, California

for

GEORGE C. MARSHALL SPACE FLIGHT CENTER
NATIONAL AERONAUTICS AND SPACE ADMINISTRATION

REPORT NO. P73-282

# DEVELOPMENT OF PORCELAIN ENAMEL PASSIVE THERMAL CONTROL COATINGS

FINAL REPORT

H. Levin
W. E. Lent
D. H. Buettner

SEPTEMBER 1973



(DCN1–2–50–23682)

Prepared under Contract No. NAS8-27439 by
HUGHES AIRCRAFT COMPANY
Culver City, California

for

GEORGE C. MARSHALL SPACE FLIGHT CENTER
NATIONAL AERONAUTICS AND SPACE ADMINISTRATION

# FOREWORD

This report is a summary of work performed on NASA contract NAS8-27439 during the period 1 July 1972 to 20 July 1973. This development effort was conducted for the George C. Marshall Space Flight Center, Huntsville, Alabama. The Contracting Officer's Technical Representative was Mr. Alden Smock, Materials Division.

The work was performed within the Materials Applications Department of the Hughes Aircraft Company under the management of Mr. Glenn L. Robinson. Mr. David H. Buettner was project engineer, with Mr. Herman Levin and Mr. William E. Lent major contributors.

Other Hughes personnel contributing to this effort included Mr. Jose Flores, Mrs. Betty Kehoe, Mr. Lonn Morris, and Mr. Byron Auker. Appreciation is herewith expressed to the following members of various commercial and academic laboratories for their helpful advice and use of special facilities:

Mr. Jerry Asmondy (Ferro Corp., Los Angeles plant)
Dr. Carl E. Frahme (Interpace Corp., Glendale Research Center)
Mr. William E. Gardner (Sloan Research Industries)
Mr. Carl Jones (Interpace Corp., Glendale Research Center)
Dr. Glenn H. Mc Intyre (Tizon Chemical Corp.)
Dr. John D. Mackenzie (U.C.L.A., Materials Science Dept.)
Mr. William H. Payne (Solid State Electronics)

**Preceding page blank**

## ABSTRACT


A white porcelain enamel coating was developed for application to high temperature metallic alloy substrates on spacecraft. The coating consists of an optically opacifying zirconia pigment, a lithia-zirconia-silica frit, and an inorganic pigment dispersant. The coating is fired at 1000° to 1150°C to form the enamel. The coating has a solar absorptance ($\alpha_s$) of 0.22 and a total normal emittance of 0.82 for a 0.017 cm thick coating and exhibits a $\Delta\alpha_s = 0.04$ after 1000 equivalent solar hours of ultraviolet radiation. The coating exhibits excellent adhesion, cleanability, and integrity and is thermal shock resistant to 900°C. Capability to coat large panels has been demonstrated by successful coating of 30 cm x 30 cm Hastelloy X alloy panels.

Preliminary development of low temperature enamels for application to aluminum and titanium alloy substrates was initiated. It was determined that both leaded and leadless frits were feasible when applied with appropriate mill fluxes. Indications were that opacification could be achieved at firing temperatures below 540°C for extended periods of time.


**Preceding page blank**

CONTENTS



**Preceding page blank**

Preceding page blank

ILLUSTRATIONS

ILLUSTRATIONS (Continued)

ILLUSTRATIONS (Continued)



LIST OF TABLES

## 1.0 INTRODUCTION

One of the major areas of technology associated with development of the space shuttle is the Thermal Protection System of the orbiter. This system must survive transient temperatures of up to 1400°C (2500°F) during boost and entry, provide a surface that will radiatively control temperature during orbital flight, and withstand the effects of the space and terrestrial environments. Although a ceramic tile reusable surface insulation system will be used for large areas, there is also a need for a high temperature resistant coating to be applied to metallic substrates. This investigation was directed toward a white porcelain enamel that is compatible with all the environments. The coating must therefore have a low solar absorptance and a high thermal emittance. The coating must maintain these properties through severe environmental constraints including re-entry heating, dust, rain, salt-spray, other earth contaminants and orbital radiation (solar ultraviolet radiation). It must also be easily cleanable, restoring the coating thermal optical properties following each mission. The coating must also maintain physical integrity when applied to different metallic substrates and exposed to severe thermal cycles. Finally, the coating system must be tailored to process limitations imposed when using various metallic substrates.

During this second year of work, the main effort was directed toward completion of the high temperature enamel development and demonstration of its process scale-up. The time consumption for this task was large. Hence only a preliminary effort could be mounted with regard to low temperature enamel development. Such low temperature enamels are designed for coating appropriate aluminum (maximum enameling temperature ≈ 475 - 550°C) or titanium (maximum enameling temperature ≈ 700 - 760°C) alloys.

Development of high temperature enamels (designated HFE – herein) involved a major frit (glass) development effort. Each frit was screened first for selective crystallization potential. Subsequently the crystallized frit was evaluated as a dispersion medium in which submicron zirconia pigment could be distributed and fired to a coherent, adherent enamel displaying optimum opacity to the solar spectrum. Over 550 enameled specimens were evaluated to consider the effects of frit formulation opacifiers, processing methods, and firing schedules on enamel properties, particularly opacification.

Low temperature enamel studies included a preliminary comparison of several commercial frits with selected experimental frits.

English units were used during the work. These have been converted to the SI system of units.

## 2.0 SUMMARY

The objective of this program has been the development of porcelain enamel passive thermal control coatings, including a high temperature category (1000-1200°C) appropriate for superalloys and a low temperature category (500-700°C) designed for aluminum or titanium alloys.

Optimization and process scale-up of high temperature enamels has been completed, and the results may be summarized as follows:

1. High temperature, zirconia-pigmented, zirconia containing enamels have been coated on Hastelloy X at temperatures as high as 1150°C. These exhibit good adhesion, good cleanability, and good coating integrity.

2. Initial solar absorptance ($\alpha_s$) values of these enamels (as fired on Hastelloy X) range from 0.31 for a thickness of 0.0089 cm (0.0035 in.) to 0.22 for a thickness of 0.0165 cm (0.0065 in.).

3. Exposure of such enameled Hastelloy X to 983 equivalent solar hours (ESH) of UV irradiation from a Xenon lamp causes the above $\alpha_s$ values to increase from 0.22 to 0.26 and from 0.31 to 0.34. A $\Delta\alpha_s \approx 0.03 - 0.04$ appears to be typical and independent of enamel thickness.

4. Repeated thermal cycling of the enamels from 20-900°C at rates of the order of 20-25°C/sec causes a rise in $\alpha_s$ from 0.24 to 0.30. Except for a blistering tendency, correctible by reduced flux content in the frit composition, adhesion and enamel integrity are unaffected.

5. Scale-up in materials preparation and enameling has been demonstrated with 30 cm x 30 cm x 0.122 cm (12 in. x 12 in. x 0.049 in.) panels of Hastelloy X. Depending on enamel used, warpage of the order of 0.4 cm was observed with a 0.01 cm enamel thickness on a 0.122 cm substrate. This is considered reasonable.

6. Important material and processing developments are as follows:

Frit Selection and Preparation

- Glasses prepared from the system $Li_2O$ - $ZrO_2$ - $SiO_2$ are very attractive for high temperature frits. They offer good crystallization potential (for opacity) and good enameling properties. Molar compositions may range from (a) $Li_2O$ - $ZrO_2$ - 4 $SiO_2$ to (b) $Li_2O$ - $ZrO_2$ - 1.3 $SiO_2$, with minor amounts ($\leq 5$ mole % each) of alumina, alkali fluorides, and $B_2O_3$, and minor to moderate amounts of alkali and alkaline earth oxides ($\leq 10$ mole % each).
- The flux components in the frit are critical to enameling properties. These require further definition but are tentatively identified as follows:

$$B_2O_3/ZrO_2 \leq 0.5$$

$$F^-/ZrO_2 \leq 0.2$$

Total Alkali Flux/$ZrO_2 \approx 1.4$ to 1.6

Total Flux/$ZrO_2 \approx 2.5$ to 3.0

- Frits with zirconia contents $> 10$ mole % are preferred because of their greater potential opacification contribution.
- Frit composition and smelting should be such as to produce a glass with negligible outgassing upon refiring to enameling temperatures (1000-1200°C) or service temperatures (900-1000°C). Failure in this regard negates opacification efforts and impairs resistance to thermal cycling at service temperatures.

Frit Crystallization

- Under conditions selective for zirconium, preferential zircon crystallization occurs in frits with high silica contents (see above) and zirconia with low silica contents (see above).
- Zircon/zirconia crystallization in large frit grains (bulk) critically depends on the nucleating agent in some minimum concentration. Such species selective crystallization proved difficult to induce within the glass mass and was only observed with $MgF_2$ (HF-39-1) at a minimum concentration of 5 mole %. $TiO_2$, a well known nucleating agent, proved ineffective for preferential zircon/zirconia crystallization (HF-34-1).

- Crystallization of high surface/volume ratio frit powders (1-40 micron) is apparently catalyzed by grain surface defects or constituents and is relatively independent of nucleating agent (see HF-34-1 versus -2). Such surface nucleation and crystallization provides a convenient and effective technique for frit powders of size < 325 mesh (<~44 microns).

Pigment Selection

- Submicron zirconia is used as a refractory, optically effective, opacifying pigment. A size range distributed about 0.5-0.7 microns represents an acceptable compromise between optimum opacification (0.2-0.3 micron) and improved firing properties of the enamel (>1 micron). The cubic phase of zirconia is used to gain high thermal expansion (i.e., to improve expansion match with the superalloy substrate). Yttria is specified as the stabilizer for the cubic phase because of its inertness at high temperature to silica, the chief frit component.

Slip Formulation

- Optimum slip formulation involves a minimum of mill additives. Besides the pigment, sodium hexametaphosphate is used to promote dispersion of the colloidal pigment and "coarse" zircon (-200 mesh) to promote bisque toughness. The water content is adjusted for a specific gravity ≈ 1.60-1.70 and a viscosity suitable for spray application with a given gun. A two coat spray application with firing after each coat seems to offer the best processing flexibility.

Enameling

- Depending on the enamel, small panels (≤ 10 cm x 10 cm) fired satisfactorily at 1000-1150°C within 30-45 seconds. Larger panels with similar coatings were enameled at these temperatures within 60-90 seconds.

Low temperature enamel development (e.g., for aluminum and titanium alloys) was also initiated this past year. Preliminary studies with commercial and experimental frits on type 6061 aluminum alloy indicated that lead-free as well as the more conventional leaded frits are feasible when applied with appropriate mill fluxes, e.g., Al-30 (Ferro Corp.). Limited pigmentation efforts with a rutile mill addition indicated that such opacification was best served by enameling at lower temperature (≤ 540°C) for extended periods of time.

## 3.0 HIGH TEMPERATURE ENAMELS FOR THERMAL CONTROL

Opacification (to the solar spectrum) has been found to be the controlling parameter in this high temperature enamel development. Property trade-offs must necessarily acknowledge this fact. Poor results can often result when subtle (but damaging) effects on opacity are not recognized. For example, optimum introduction of optical back scatterers (via frit crystallization and mill-added pigmentation) can be largely negated by enamel defects. Thus, hairline tearing and/or excess bubble structure in the enamel "reveal" the dark, oxidized substrate and depress the opacity severely. Such effects are exaggerated in the thin ($\leq 0.01$ cm), super opaque ($\alpha_S \approx 0.2$) coatings being sought. Enamel development was therefore pursued in an iterative manner involving: (1) frit preparation and processing, (2) combined frit/pigment evaluation in enamels, (3) preparation and processing of modified frits, (4) re-evaluation of the modified frit with pigment in enamels etc.

Mill pigmentation of an uncrystallized frit (HF-2; see report of first year's work[1]) reveals a limit of an order of 32 percent by weight ($\sim 18$ percent by volume) zirconia addition before enamel quality becomes unacceptable. Such pigmentation with yttria-stabilized, submicron zirconia yields a mat (non-glossy) enamel with solar absorptance ($\alpha_s$) $\approx 0.26$ as fired at 970-990°C to a thickness $\approx 0.011$ cm (0.0044 in.) on Hastelloy X. Such high pigmentation places tight constraints upon enameling to prevent defect generation. In an effort to reduce reliance on mill pigmentation for opacification, an extensive investigation of pre-crystallized frits was undertaken. Achievement of <u>controlled</u> crystallization in the frit prior to incorporation in the enamel formulation permits the phase separation of crystallites,

**Preceding page blank**

selective as to species, size range, and uniformity of distribution in the glass host. The net effect is a separate opacification of the glass frit prior to its use in incorporating a pigment phase in the enamel. It was considered that such complementary opacification would reduce dependence on mill-added opacifiers and thus provide an enamel of increased glass content with attendant, superior mechanical properties. An added advantage would be a decrease in tearing, hairlining and application difficulty.

## 3.1 EXPERIMENTAL WORK

### 3.1.1 Frit Design and Preparation

The mechanical properties of a porcelain enamel primarily are determined by the properties of the parent frit or glass used in its preparation. Such being the case, requisite frit and enamel properties are quite similar, and for this high temperature coating development, desirable frit properties are as follows:

- High fusion temperature range (900-1300$^{\circ}$C)
- High linear thermal expansion ($\geq 140 \times 10^{-7}/^{\circ}C$)
- High opacification potential via controlled crystallization at temperatures $\geq\sim 900^{\circ}C$
- Good resistance to thermal- and UV-degradation of optical and mechanical properties
- Good enamel integrity and surface finish to promote cleanability
- Free as possible from gas bubbles. (Complete fining)

The fusion range is defined by consideration of several benchmark temperatures as follows:

- Practical upper limit of glass smelting $\approx 1600^{\circ}C$. Reference is to resistance- or gas-heated as opposed to induction-heated furnaces. The smelting crucible is the main limiting factor.
- Maximum service temperature of superalloy substrates is an order of 1100$^{\circ}$C.
- Maximum allowable enameling temperature is an order of 1100-1300$^{\circ}$C.

These relatively high temperatures indicate the need for a refractory glass. High silica content borosilicate, alumino-silicate, or zirconium silicate glass appears applicable.

Linear thermal contraction of most of the superalloys exceeds $150 \times 10^{-7}/^{o}C$ in the cooling interval between a typical glass annealing point (viscosity = $10^{13}$ poise; say 500-700$^{o}$C) and room temperature. Glass linear expansion ($\alpha_T$) preferably should be near but slightly below the metal value so as to introduce a small compressive stress. Flux selection has an important bearing on $\alpha_T$ as indicated in the following normalized values[2, 3] of alkali and alkaline earth fluxes and $B_2O_3$:

| Relative $\alpha_T$ Factor | |
|---|---|
| $Li_2O$ | 138 |
| $Na_2O$ | 100 |
| $K_2O$ | 77 |
| CaO | 50 |
| BaO | 30 |
| ZnO | 21 |
| MgO | 1 |
| $B_2O_3$ | 1 |

The relatively high $\alpha_T$ value required to match that of the metal substrate thus requires a major alkali flux content, say > 20 mole percent depending on refractory content. For purposes of broadening the maturing range, lesser contents of CaO/BaO look attractive. The $B_2O_3$ content should be requisite for glass formation (i. e. , together with $SiO_2/Al_2O_3$).

Zircon and zirconia are relatively insoluble in glass at moderate temperature. Further their melting points greatly exceed enameling or enamel service temperatures. Their indexes of refraction are approximately 2. 0 and 2. 2, respectively. These properties coupled with the need for a powerful flux content (see above) combine to make zirconium crystallizing frits look both practical and very attractive in terms of opacification potential.

UV-discoloration effects are often related to certain impurities, especially titanium in the presence of other transition elements. Avoidance of these ions as impurities or as parent materials during formulation and processing is beneficial. Thermal degradation and maintenance of enamel integrity are intimately related to frit design and enamel formulation and processing as discussed later.

Two primary glass forming systems were investigated: $Li_2O$ - $ZrO_2$ - $SiO_2$ and $Li_2O$ - $B_2O_3$ - $ZrO_2$ - $SiO_2$. When supplemented by other minor additions of alkali and alkaline earth fluxes for improved enameling and $F^-/Al_2O_3$ for nucleation, the latter system proved more attractive. The system $Li_2O$ - $Na_2O$ - $CaO$ - $B_2O_3$ - $ZrO_2$ - $SiO_2$ appears to have real potential, but time permitted only limited investigation. Data on these and related lithium zirconium silicate systems is limited. However some guidance is available from the Russian literature[4, 5, 6], Jacobs[7, 8], Oel et. al[9], and Sawai[10].

An order of 50 frits were formulated as modifications of the above zirconia glass systems. Most of these are presented in Tables 1, 2, and 3. Powder charges (for melting) were hand-blended from reagent grade oxides, carbonates, and fluorides. Melting (in 100 g batches) was carried out in a small gas/air-fired Bickley kiln at 1525-1550°F for ~ 20 minutes, using heavy wall fireclay crucibles (Denver Fire Clay No. 990-210-02). Some crucible attack (with resultant batch contamination) and loss of flux (volatilization and crucible reaction) were accepted as inevitable during this lab-screening of experimental frits.

The frits are arranged in the tables as three groups: low zirconia (< 10 percent by weight), medium zirconia (10-20 percent by weight), and high zirconia (> 20 percent by weight). Comments pertinent to these data are as follows:

- Fluorides

  Added individually or in combination primarily for nucleation of zircon and/or zirconia during post-smelt crystallization. Selected on basis of m. p. > crystal growth temperature, reduced solubility in glass at 500-600°C, and where possible a crystal form match to zircon (tetragonal) or zirconia

TABLE 1. ESTIMATED MELTED COMPOSITIONS OF EXPERIMENTAL CRYSTALLIZING FRITS — LOW ZIRCONIA CONTENT

| Component Oxide | HF-46 | | HF-25 | | HF-27 | | HF-29 | |
|---|---|---|---|---|---|---|---|---|
| | Mole % | Wt. % | Mole % | Wt. % | Mole % | Wt. % | Mole % | Wt. % |
| $SiO_2$ | 44.0 | 44.6 | 53.2 | 46.2 | 46.1 | 39.4 | 43.4 | 37.0 |
| $ZrO_2$ | 4.0 | 8.3 | 5.2 | 9.3 | 5.2 | 9.1 | 5.2 | 9.0 |
| $Al_2O_3$ | 1.0 | 1.7 | 6.5 | 9.6 | 7.7 | 11.1 | 10.4 | 15.0 |
| $B_2O_3$ | 14.0 | 16.2 | 9.1 | 9.1 | 15.0 | 14.9 | 11.2 | 11.0 |
| $Li_2O$ | 14.0 | 7.0 | 8.6 | 3.7 | 8.6 | 3.7 | 4.7 | 2.0 |
| $Na_2O$ | 8.0 | 8.4 | - | - | - | - | 1.1 | 1.0 |
| CaO | 12.0 | 11.6 | 1.0 | 0.8 | 1.0 | 0.8 | 15.1 | 12.0 |
| BaO | - | - | 7.8 | 17.3 | 7.8 | 17.1 | 4.6 | 10.0 |
| LiF | 1.0 | 0.4 | 5.2 | 2.0 | 5.2 | 1.9 | - | - |
| NaF | 1.0 | 0.7 | 3.4 | 2.0 | 3.4 | 2.0 | 3.4 | 2.0 |
| $MgF_2$ | 1.0 | 1.1 | - | - | - | - | - | - |
| $CaF_2$ | - | - | - | - | - | - | - | - |
| ZnO | - | - | - | - | - | - | 0.9 | 1.0 |
| $SnO_2$ | - | - | - | - | - | - | - | - |
| $TiO_2$ | - | - | - | - | - | - | - | - |
| TOTAL | 100.0 | 100.0 | 100.0 | 100.0 | 100.0 | 100.0 | 100.0 | 100.0 |
| Mole Ratio: | | | | | | | | |
| Alkali Flux/ $ZrO_2$ | 6.0 | | 3.3 | | 3.3 | | 1.8 | |
| $B_2O_3/ZrO_2$ | 3.5 | | 1.8 | | 2.9 | | 2.2 | |
| Total Flux*/ $ZrO_2$ | 12.8 | | 6.8 | | 7.9 | | 7.9 | |

*Includes $B_2O_3$, fluorides and ZnO

TABLE 2. ESTIMATED MELTED COMPOSITIONS OF EXPERIMENTAL CRYSTALLIZING FRITS – MEDIUM ZIRCONIA CONTENT

| Component Oxide | HF-26 | | HF-28 | | HF-40 | | HF-24 | |
|---|---|---|---|---|---|---|---|---|
| | Mole % | Wt. % | Mole % | Wt. % | Mole % | Wt. % | Mole % | Wt. % |
| $SiO_2$ | 45.6 | 38.4 | 54.8 | 50.0 | 50.5 | 43.6 | 52.5 | 45.0 |
| $ZrO_2$ | 6.8 | 11.8 | 6.9 | 13.0 | 7.0 | 12.4 | 7.1 | 12.5 |
| $Al_2O_3$ | 7.6 | 10.8 | 2.6 | 4.0 | 4.0 | 5.8 | 6.1 | 8.8 |
| $B_2O_3$ | 14.7 | 14.4 | 15.2 | 16.0 | 7.9 | 7.9 | 7.9 | 7.9 |
| $Li_2O$ | 8.3 | 3.5 | 4.4 | 2.0 | 11.1 | 4.8 | 8.9 | 3.8 |
| $Na_2O$ | - | - | 2.1 | 2.0 | 5.6 | 5.0 | - | - |
| CaO | 1.0 | 0.8 | 8.2 | 7.0 | 1.0 | 0.8 | 1.0 | 0.8 |
| BaO | 7.6 | 16.4 | 0.9 | 2.0 | 7.9 | 17.4 | 7.9 | 17.3 |
| LiF | 5.1 | 1.9 | - | - | 3.0 | 1.1 | 5.2 | 1.9 |
| NaF | 3.3 | 2.0 | 3.2 | 2.0 | 2.0 | 1.2 | 3.4 | 2.0 |
| $MgF_2$ | - | - | - | - | - | - | - | - |
| $CaF_2$ | - | - | - | - | - | - | - | - |
| ZnO | - | - | 1.7 | 2.0 | - | - | - | - |
| $SnO_2$ | - | - | - | - | - | - | - | - |
| $TiO_2$ | - | - | - | - | - | - | - | - |
| TOTAL | 100.0 | 100.0 | 100.0 | 100.0 | 100.0 | 100.0 | 100.0 | 100.0 |
| Mole Ratio: | | | | | | | | |
| Alkali Flux/ $ZrO_2$ | 2.5 | | 1.4 | | 3.1 | | 2.5 | |
| $B_2O_3/ZrO_2$ | 2.2 | | 2.2 | | 1.1 | | 1.1 | |
| Total Flux*/ $ZrO_2$ | 5.9 | | 5.2 | | 5.5 | | 4.8 | |

(Table 2, continued)

| Component Oxide | HF-44 | | HF-33 | | HF-34 | | HF-30 | |
|---|---|---|---|---|---|---|---|---|
| | Mole % | Wt. % | Mole % | Wt. % | Mole % | Wt. % | Mole % | Wt. % |
| $SiO_2$ | 51.2 | 45.0 | 54.6 | 45.0 | 46.9 | 38.0 | 50.0 | 43.9 |
| $ZrO_2$ | 7.1 | 12.8 | 7.1 | 12.0 | 7.2 | 12.0 | 7.5 | 13.5 |
| $Al_2O_3$ | 3.0 | 4.5 | 5.8 | 8.0 | 7.3 | 10.0 | 4.0 | 6.0 |
| $B_2O_3$ | 7.9 | 8.0 | 9.4 | 9.0 | 16.0 | 15.0 | 7.9 | 8.1 |
| $Li_2O$ | 8.9 | 3.9 | 9.8 | 4.0 | 9.9 | 4.0 | 8.9 | 3.9 |
| $Na_2O$ | - | - | - | - | - | - | - | - |
| CaO | 1.0 | 0.8 | 1.3 | 1.0 | 1.3 | 1.0 | 1.0 | 0.8 |
| BaO | 7.9 | 17.7 | 7.6 | 16.0 | 7.7 | 16.0 | 7.9 | 17.7 |
| LiF | 10.0 | 3.8 | - | - | - | - | 7.8 | 3.0 |
| NaF | - | - | - | - | - | - | 5.0 | 3.1 |
| $MgF_2$ | - | - | - | - | - | - | - | - |
| $CaF_2$ | - | - | - | - | - | - | - | - |
| ZnO | - | - | 4.4 | 5.0 | - | - | - | - |
| $SnO_2$ | - | - | - | - | - | - | - | - |
| $TiO_2$ | 3.0 | 3.5 | - | - | 3.7 | 4.0 | - | - |
| TOTAL | 100.0 | 100.0 | 100.0 | 100.0 | 100.0 | 100.0 | 100.0 | 100.0 |
| Mole Ratio: | | | | | | | | |
| Alkali Flux/ $ZrO_2$ | 2.7 | | 1.4 | | 1.4 | | 2.9 | |
| $B_2O_3/ZrO_2$ | 1.1 | | 1.3 | | 2.2 | | 1.1 | |
| Total Flux*/ $ZrO_2$ | 5.0 | | 4.6 | | 4.9 | | 5.1 | |

(Table 2, continued)

| Component Oxide | HF-31 | | HF-42 | | HF-43 | | HF-23 | |
|---|---|---|---|---|---|---|---|---|
| | Mole % | Wt. % | Mole % | Wt. % | Mole % | Wt. % | Mole % | Wt. % |
| $SiO_2$ | 49.5 | 43.3 | 50.3 | 43.7 | 48.3 | 42.7 | 50.7 | 51.9 |
| $ZrO_2$ | 8.0 | 14.3 | 8.0 | 14.3 | 8.0 | 14.5 | 8.2 | 17.2 |
| $Al_2O_3$ | 4.0 | 6.0 | 3.0 | 4.4 | 3.0 | 4.5 | 5.3 | 9.2 |
| $B_2O_3$ | 7.9 | 8.0 | 7.9 | 8.0 | 7.9 | 8.1 | - | - |
| $Li_2O$ | 8.9 | 3.9 | 8.9 | 3.9 | 8.9 | 3.9 | 11.6 | 5.9 |
| $Na_2O$ | - | - | - | - | - | - | - | - |
| CaO | 1.0 | 0.8 | 1.0 | 0.8 | 1.0 | 0.8 | - | - |
| BaO | 7.9 | 17.7 | 7.9 | 17.6 | 7.9 | 17.9 | - | - |
| LiF | 7.8 | 2.9 | 10.0 | 3.8 | 10.0 | 3.8 | 15.8 | 7.0 |
| NaF | 5.0 | 3.1 | - | - | 2.5 | 1.5 | 6.2 | 4.4 |
| $MgF_2$ | - | - | - | - | 2.5 | 2.3 | - | - |
| $CaF_2$ | - | - | - | - | - | - | - | - |
| ZnO | - | - | - | - | - | - | - | - |
| $Li_3PO_4$ | - | - | - | - | - | - | 2.2 | 4.4 |
| $TiO_2$ | - | - | 3.0 | 3.5 | - | - | - | - |
| TOTAL | 100.0 | 100.0 | 100.0 | 100.0 | 100.0 | 100.0 | 100.0 | 100.0 |
| Mole Ratio: | | | | | | | | |
| Alkali Flux/ $ZrO_2$ | 2.7 | | 2.4 | | 2.7 | | 4.1 | |
| $B_2O_3/ZrO_2$ | 1.0 | | 1.0 | | 1.0 | | --- | |
| Total Flux* / $ZrO_2$ | 4.8 | | 4.5 | | 5.1 | | 4.1 | |

(Table 2, continued)

| Component Oxide | HF-17 | | HF-18 | | HF-32 | | HF-20 | |
|---|---|---|---|---|---|---|---|---|
| | Mole % | Wt. % | Mole % | Wt. % | Mole % | Wt. % | Mole % | Wt. % |
| $SiO_2$ | 51.0 | 46.0 | 51.0 | 45.0 | 49.0 | 42.7 | 54.0 | 52.1 |
| $ZrO_2$ | 8.5 | 15.7 | 8.5 | 15.4 | 8.5 | 15.2 | 9.0 | 17.8 |
| $Al_2O_3$ | 8.5 | 14.3 | 8.5 | 13.9 | 4.0 | 5.9 | 4.5 | 7.4 |
| $B_2O_3$ | 15.0 | 15.8 | 15.0 | 15.4 | 7.9 | 8.0 | 10.0 | 11.2 |
| $Li_2O$ | 8.5 | 3.8 | 8.5 | 3.7 | 8.9 | 3.9 | 9.0 | 4.3 |
| $Na_2O$ | - | - | - | - | - | - | - | - |
| CaO | - | - | - | - | 1.0 | 0.8 | - | - |
| BaO | - | - | - | - | 7.9 | 17.6 | - | - |
| LiF | 4.3 | 1.7 | 6.0 | 2.3 | 7.8 | 2.9 | 7.2 | 3.0 |
| NaF | 4.2 | 2.7 | - | - | 5.0 | 3.0 | 6.3 | 4.2 |
| $MgF_2$ | - | - | - | - | - | - | - | - |
| $CaF_2$ | - | - | - | - | - | - | - | - |
| ZnO | - | - | - | - | - | - | - | - |
| $Li_3PO_4$ | - | - | 2.5 | 4.3 | - | - | - | - |
| $TiO_2$ | - | - | - | - | - | - | - | - |
| TOTAL | 100.0 | 100.0 | 100.0 | 100.0 | 100.0 | 100.0 | 100.0 | 100.0 |
| Mole Ratio: | | | | | | | | |
| Alkali Flux/ $ZrO_2$ | 2.0 | | 2.0 | | 2.6 | | 2.5 | |
| $B_2O_3/ZrO_2$ | 1.8 | | 1.8 | | 0.9 | | 1.1 | |
| Total Flux*/ $ZrO_2$ | 3.8 | | 3.8 | | 4.5 | | 3.6 | |

(Table 2, continued)

| Component Oxide | HF-21 | | HF-35 | | HF-36 | | HF-37 | |
|---|---|---|---|---|---|---|---|---|
| | Mole % | Wt. % | Mole % | Wt. % | Mole % | Wt. % | Mole % | Wt. % |
| $SiO_2$ | 54.0 | 50.9 | 48.5 | 42.1 | 48.5 | 41.0 | 48.5 | 41.0 |
| $ZrO_2$ | 9.0 | 17.4 | 9.0 | 16.0 | 9.0 | 15.6 | 9.0 | 15.6 |
| $Al_2O_3$ | 4.5 | 7.2 | 4.0 | 5.9 | 4.0 | 5.7 | 4.0 | 5.7 |
| $B_2O_3$ | 10.0 | 10.9 | 7.9 | 8.0 | 7.9 | 7.7 | 7.9 | 7.7 |
| $Li_2O$ | 9.0 | 4.2 | 8.9 | 3.8 | 8.9 | 3.7 | 8.9 | 3.7 |
| $Na_2O$ | - | - | - | - | - | - | - | - |
| CaO | - | - | 1.0 | 0.8 | 1.0 | 0.8 | 1.0 | 0.8 |
| BaO | - | - | 7.9 | 17.5 | 7.9 | 17.2 | 7.9 | 17.0 |
| LiF | 10.8 | 4.4 | 7.8 | 2.9 | 7.8 | 2.8 | 7.8 | 2.8 |
| NaF | - | - | 5.0 | 3.0 | - | - | - | - |
| $MgF_2$ | - | - | - | - | - | - | - | - |
| $CaF_2$ | - | - | - | - | 5.0 | 5.5 | - | - |
| ZnO | - | - | - | - | - | - | 5.0 | 5.7 |
| $Li_3PO_4$ | 2.7 | 5.0 | - | - | - | - | - | - |
| $TiO_2$ | - | - | - | - | - | - | - | - |
| TOTAL | 100.0 | 100.0 | 100.0 | 100.0 | 100.0 | 100.0 | 100.0 | 100.0 |
| Mole Ratio: | | | | | | | | |
| Alkali Flux/ $ZrO_2$ | 2.5 | | 2.4 | | 1.9 | | 1.9 | |
| $B_2O_3/ZrO_2$ | 1.1 | | 0.9 | | 0.9 | | 0.9 | |
| Total Flux*/ $ZrO_2$ | 3.6 | | 4.3 | | 4.3 | | 4.3 | |

(Table 2, continued)

| Component Oxide | HF-38 | | HF-39 | | HF-41 | | HF-2 | |
|---|---|---|---|---|---|---|---|---|
| | Mole % | Wt. % | Mole % | Wt. % | Mole % | Wt. % | Mole % | Wt. % |
| $SiO_2$ | 48..5 | 39.0 | 48.5 | 41.6 | 48.5 | 41.1 | 46.6 | 41.0 |
| $ZrO_2$ | 9.0 | 14.8 | 9.0 | 15.8 | 9.0 | 15.6 | 9.8 | 17.7 |
| $Al_2O_3$ | 4.0 | 5.5 | 4.0 | 5.8 | 4.0 | 5.7 | 4.0 | 6.0 |
| $B_2O_3$ | 7.9 | 7.4 | 7.9 | 7.8 | 7.9 | 7.8 | 6.8 | 6.8 |
| $Li_2O$ | 8.9 | 3.5 | 8.9 | 3.8 | 11.1 | 4.7 | - | - |
| $Na_2O$ | - | - | - | - | 5.6 | 4.9 | 6.6 | 6.0 |
| CaO | 1.0 | 0.8 | 1.0 | 0.8 | 1.0 | 0.8 | 1.2 | 1.0 |
| BaO | 7.9 | 16.2 | 7.9 | 17.3 | 7.9 | 17.1 | 4.2 | 9.5 |
| LiF | 7.8 | 2.7 | 7.8 | 2.9 | 3.0 | 1.1 | 15.8 | 6.0 |
| NaF | - | - | - | - | 2.0 | 1.2 | - | - |
| $MgF_2$ | - | - | 5.0 | 4.4 | - | - | - | - |
| $CaF_2$ | - | - | - | - | - | - | - | - |
| ZnO | - | - | - | - | - | - | 5.0 | 6.0 |
| $SnO_2$ | 5.0 | 10.1 | - | - | - | - | - | - |
| $TiO_2$ | - | - | - | - | - | - | - | - |
| TOTAL | 100.0 | 100.0 | 100.0 | 100.0 | 100.0 | 100.0 | 100.0 | 100.0 |
| Mole Ratio: | | | | | | | | |
| Alkali Flux/ $ZrO_2$ | 1.9 | | 1.9 | | 2.4 | | 2.3 | |
| $B_2O_3/ZrO_2$ | 0.9 | | 0.9 | | 0.9 | | 0.7 | |
| Total Flux*/ $ZrO_2$ | 3.7 | | 4.3 | | 4.3 | | 4.0 | |

(Table 2, concluded)

| Component Oxide | HF-6 | | HF-10 | | HF-47 | | | |
|---|---|---|---|---|---|---|---|---|
| | Mole % | Wt. % | Mole % | Wt. % | Mole % | Wt. % | | |
| $SiO_2$ | 60.0 | 56.2 | 60.0 | 58.7 | 42.0 | 39.7 | | |
| $ZrO_2$ | 10.0 | 19.2 | 10.0 | 20.1 | 10.0 | 19.3 | | |
| $Al_2O_3$ | 10.0 | 15.9 | 5.0 | 8.3 | - | - | | |
| $B_2O_3$ | - | - | - | - | 8.0 | 8.8 | | |
| $Li_2O$ | 10.0 | 4.7 | 10.0 | 4.9 | 7.0 | 3.3 | | |
| $Na_2O$ | - | - | - | - | 6.0 | 5.9 | | |
| CaO | - | - | - | - | 10.0 | 9.0 | | |
| BaO | - | - | - | - | - | - | | |
| LiF | 10.0 | 4.0 | 8.0 | 3.4 | 9.0 | 3.7 | | |
| NaF | - | - | 7.0 | 4.6 | - | - | | |
| $MgF_2$ | - | - | - | - | - | - | | |
| $CaF_2$ | - | - | - | - | - | - | | |
| ZnO | - | - | - | - | 8.0 | 10.3 | | |
| $SnO_2$ | - | - | - | - | - | - | | |
| $TiO_2$ | - | - | - | - | - | - | | |
| TOTAL | 100.0 | 100.0 | 100.0 | 100.0 | 100.0 | 100.0 | | |
| Mole Ratio: | | | | | | | | |
| Alkali Flux/ $ZrO_2$ | 2.0 | | 2.5 | | 2.2 | | | |
| $B_2O_3/ZrO_2$ | --- | | --- | | 0.8 | | | |
| Total Flux*/ $ZrO_2$ | 2.0 | | 2.5 | | 4.8 | | | |

*Includes $B_2O_3$, fluorides, and ZnO

TABLE 3. ESTIMATED MELTED COMPOSITIONS OF EXPERIMENTAL CRYSTALLIZING FRITS — HIGH ZIRCONIA CONTENT

| Component Oxide | HF-22 | | HF-54 | | HF-45 | | HF-49 | |
|---|---|---|---|---|---|---|---|---|
| | Mole % | Wt. % | Mole % | Wt. % | Mole % | Wt. % | Mole % | Wt. % |
| $SIO_2$ | 51.9 | 52.8 | 51.7 | 46.5 | 47.0 | 42.2 | 40.0 | 36.3 |
| $ZrO_2$ | 10.3 | 21.5 | 11.8 | 21.8 | 12.0 | 21.9 | 12.0 | 22.3 |
| $Al_2O_3$ | 5.1 | 8.9 | 3.3 | 5.0 | 3.0 | 4.5 | 2.0 | 3.1 |
| $B_2O_3$ | - | - | 5.4 | 5.6 | 9.0 | 9.5 | 15.0 | 15.8 |
| $Li_2O$ | 11.3 | 5.7 | 10.5 | 4.7 | 12.0 | 5.4 | - | - |
| $Na_2O$ | - | - | 5.9 | 5.4 | 6.0 | 5.6 | 7.0 | 6.6 |
| CaO | - | - | 5.1 | 4.3 | 5.0 | 4.2 | 5.0 | 4.2 |
| BaO | - | - | 2.0 | 4.6 | 2.0 | 4.6 | - | - |
| LiF | 15.4 | 6.8 | 2.2 | 0.8 | 2.0 | 0.8 | 14.0 | 5.5 |
| NaF | 6.0 | 4.3 | 2.1 | 1.3 | 2.0 | 1.3 | - | - |
| $MgF_2$ | - | - | - | - | - | - | - | - |
| $CaF_2$ | - | - | - | - | - | - | - | - |
| ZnO | - | - | - | - | - | - | 5.0 | 6.2 |
| $SnO_2$ | - | - | - | - | - | - | - | - |
| $TiO_2$ | - | - | - | - | - | - | - | - |
| TOTAL | 100.0 | 100.0 | 100.0 | 100.0 | 100.0 | 100.0 | 100.0 | 100.0 |
| Mole Ratio: | | | | | | | | |
| Alkali Flux/ $ZrO_2$ | 3.2 | | 1.8 | | 1.8 | | 1.8 | |
| $B_2O_3/ZrO_2$ | --- | | 0.5 | | 0.8 | | 1.3 | |
| Total Flux*/ $ZrO_2$ | 3.2 | | 2.8 | | 3.2 | | 3.8 | |

(Table 3, concluded)

| Component Oxide | HF-50 | | HF-51 | | HF-52 | | HF-53 | |
|---|---|---|---|---|---|---|---|---|
| | Mole % | Wt. % | Mole % | Wt. % | Mole % | Wt. % | Mole % | Wt. % |
| $SiO_2$ | 35.0 | 31.2 | 41.0 | 36.5 | 32.3 | 29.4 | 24.0 | 21.6 |
| $ZrO_2$ | 15.0 | 27.4 | 15.0 | 27.4 | 15.2 | 28.4 | 18.0 | 33.3 |
| $Al_2O_3$ | 2.0 | 3.0 | 2.0 | 3.0 | 0.6 | 0.9 | - | - |
| $B_2O_3$ | 15.0 | 15.5 | 10.0 | 10.3 | 14.2 | 15.1 | 15.0 | 15.7 |
| $Li_2O$ | - | - | 15.0 | 6.6 | 14.5 | 6.5 | 17.5 | 7.9 |
| $Na_2O$ | 7.0 | 6.4 | 6.0 | 5.5 | 8.4 | 7.8 | 10.0 | 9.3 |
| CaO | 5.0 | 4.2 | 5.0 | 4.2 | 12.7 | 10.8 | 13.0 | 11.0 |
| BaO | - | - | 2.0 | 4.5 | - | - | - | - |
| LiF | 16.0 | 6.2 | 2.0 | 0.8 | 1.0 | 0.4 | 1.2 | 0.4 |
| NaF | - | - | 2.0 | 1.2 | 1.1 | 0.7 | 1.3 | 0.8 |
| $MgF_2$ | - | - | - | - | - | - | - | - |
| $CaF_2$ | - | - | - | - | - | - | - | - |
| ZnO | 5.0 | 6.1 | - | - | - | - | - | - |
| $SnO_2$ | - | - | - | - | - | - | - | - |
| $TiO_2$ | - | - | - | - | - | - | - | - |
| TOTAL | 100.0 | 100.0 | 100.0 | 100.0 | 100.0 | 100.0 | 100.0 | 100.0 |
| Mole Ratio: | | | | | | | | |
| Alkali Flux/ $ZrO_2$ | 1.5 | | 1.7 | | 1.6 | | 1.7 | |
| $B_2O_3/ZrO_2$ | 1.0 | | 0.7 | | 0.9 | | 0.8 | |
| Total Flux*/ $ZrO_2$ | 3.2 | | 2.8 | | 3.4 | | 3.2 | |

*Includes $B_2O_3$, fluorides, and ZnO

(monoclinic). Although they can function in parallel as a powerful flux, their use in this regard should be minimized to avoid potential outgassing effects, such as those associated with reaction with the substrate and fluoride decomposition.

- $SnO_2$, $TiO_2$ (rutile), ZnO
- Alternative nucleating agents
- Frit with broad maturing range and improved mobility during firing is important to enameling and requires $Li_2O$, $Na_2O$, and CaO in combination (e.g., $2Li_2O:Na_2O:CaO$).
- Total Flux $ZrO_2$ Mole Ratio

  Enameling considerations indicate the preferred range is 2.5-3.0, depending on silica content. (Note: The total flux is designated as including $B_2O_3$, all fluorides, and ZnO.)
- Alkali Flux/$ZrO_2$ Mole Ratio

  Enameling considerations indicate the preferred range is approximately 1.4-1.6.
- $B_2O_3/ZrO_2$ Mole Ratio

  Enameling considerations indicate the preferred range is $\leq 0.5$. Values greater than 0.5 invite excess bubble structure (with resultant loss of opacity) and impose severe firing constraints in order to avoid blistering and pinhole defects in the enamel. Such defects are exaggerated when enamel firing is high enough to melt the coating and fuse hairlined areas together.

Compositional effects on frit opacification (i.e., nucleation and crystallization) are discussed in the next section.

### 3.1.2 Frit Characterization and Crystallization

Potential thermal regimes for nucleation and crystal growth were first identified by high temperature differential thermal analysis (DTA). Since this DTA technique conventionally uses a powder specimen, it is acknowledged that resultant crystal growth criteria are more descriptive of surface nucleated powders than of nucleation and crystallization in a large glass mass (i.e., termed bulk crystallization hereafter). Despite such a shortcoming, powder DTA data provide useful guidance. Based on such data, individual frit powders (of varying size ranges: 1-40 to 884-1680 microns) were subjected to varying heat treatment in air, cooled, and reground in a fused alumina mortar to -170 mesh powder. X-ray diffraction (XRD) determinations were then performed on the heat-treated powder specimens to identify crystallized phases. To a reasonable degree, these data permit correlation of crystallization with heat treatment and frit type. Further characterization of crystallite species, size range, crystal habit, and uniformity of distribution in the host glass phase was carried out by scanning electron microscope (SEM) studies. Combined DTA, XRD, and SEM data were thus used to control crystallization efforts and to direct modifications in frit composition.

3.1.2.1 Differential Thermal Analysis (DTA)

DTA thermograms for representative, untreated frit powder (< 37 micron, -400 mesh) are presented in Figures 1, 2, and 3. These were obtained from a DuPont Model 900 Thermal Analyzer with a 1600°C furnace. Determinations were made in air, using Pt macro cups and liners for both sample and reference ($Al_2O_3$) material. Liners were coated with MgO. The initial heating rate was 0.67°C/sec (40°C/min) in all cases.

Analysis of resulting thermograms yielded the estimated nucleation and crystallization data for representative frits given in Table 4. Since these DTA data were obtained with Pt liners (for reference and sample cups), the best representation of a transition temperature is the onset temperature

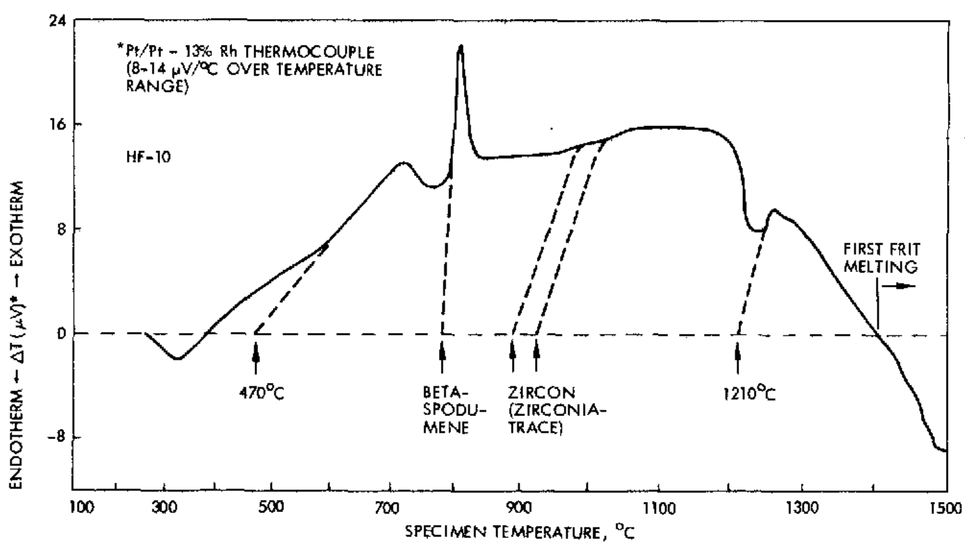


Figure 1. DTA thermogram for frit HF-10 (-400 mesh powder) — heating cycle only run at 0.67°C/sec (40°C/min)

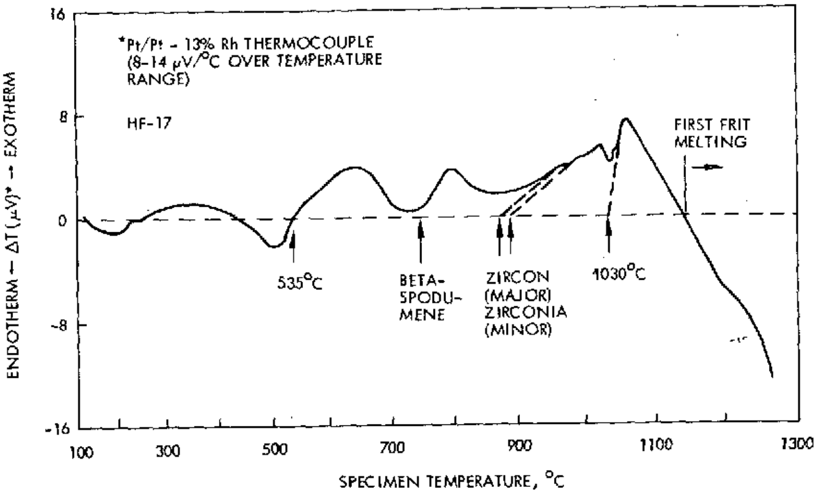


Figure 2. DTA thermogram for frit HF-17 (-400 mesh powder) — heating cycle only run at 0.67°C/sec (40°C/min)

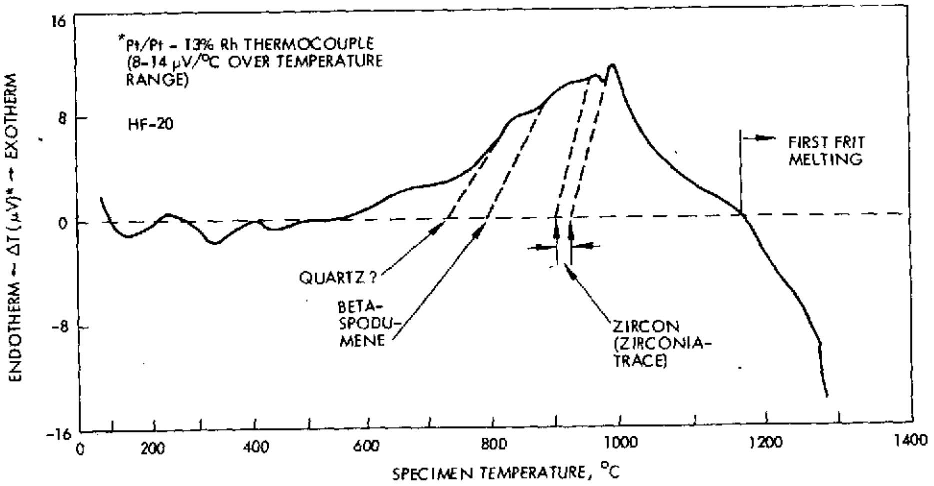


Figure 3. DTA thermogram for frit HF-20 (-400 mesh powder) — heating cycle only run at 0.67°C/sec (40°C/min)

TABLE 4. CRYSTAL TRANSITION TEMPERATURES OF TYPICAL FRITS ESTIMATED FROM DTA THERMOGRAMS

| Frit No. (Appearance) | Est. Smelt Temp. °C | Est. Nucleating Range[a] °C | Crystal Transition Temperature, °C (est.) | | | | | | |
|---|---|---|---|---|---|---|---|---|---|
| | | | ND[b] | ND[c] | ND[d] | beta-spodumene | zircon-zirconia | ND[b] | ND[b] |
| HF-2 (white opaque) | 1250-1315 | 500-550 | — | 570 | 690 | 790 | ? | ? | — |
| HF-6 (white opaque) | 1560-1595 | 500-550 | — | 550 | — | 820 | ? | — | — |
| HF-10 | 1560-1600 | 500-550 | 470 | — | — | 775 | 890 | — | — |
| HF-17 (white opaque) | 1365 1425 | 500-550 | — | 535 | — | 770 | 870 | 1000 1030 | — |
| HF-20 (translucent) | 1315-1393 | 500-550 | — | 560 | 730 | 790 | 900 920 | — | 1100 |
| HF-22 (milky) | 1540-1550 | 500-550 | — | 620 | 730 | 810 | 890 | 1040 | 1080 |
| HF-18 | 1550-1600 | 500-550 | — | 620 | — | 770 | 890 | — | 1090 1120 |
| HF-21 | 1500-1540 | 500-550 | — | ? | 740 | 790 | 900 | 1030 | — |
| HF-23 (clear) | 1350-1370 | 500-550 | 470 | 570 | 757 | 800 | 890 | 980 | — |
| HF-24 (clear) | 1560 | 490-540 | 440 | 570 | — | — | 870 | 990 1045 | — |
| HF-26 (clear) | 1520 | 490-540 | 440 | 550 | 750 (tr.) | 790 (tr.) | 870 | 970 | — |
| HF-28 (clear) | 1510 | 500-550 | 470 | 610 | — | 780 | 870 | 980 1050 | — |
| HF-25 (clear) | 1560 | 490-540 | 440 | 545 | — | 785 (tr.) | 870 933 | 1017 | — |
| HF-27 (clear) | 1530 | 490-540 | 440 | 550 | 710 757 | — | 870 923 | 1025 | — |
| HF-29 (clear) | 1510 | 500-550 | 460 | 610 | | 800 827 | 863 949 | 1030 | — |

[a]Estimated by adding 100-150°C to estimated annealing point.
[b]Not determined
[c]Possibly lithium disilicate (ref. 11)
[d]Possibly quartz (ref. 11)

(i. e., first deviation from the baseline). These onset temperatures are estimated as shown and are the estimates tabulated in Table 4. Crystal phase transition temperatures have been aligned according to temperature range in an effort to indicate similar (or identical phases) in the various frits.

#### 3.1.2.2 X-Ray Diffraction (XRD)

Each powdered specimen was packed into a micro specimen holder. X-ray diffraction spectra were obtained in a Norelco X-ray diffractometer equipped with a crystal monochromator and sample spinner. Quantitative estimates were obtained with the aid of calibration curves derived from synthetic standards made up on a weight percent basis.

The correlation of crystallization with XRD results is presented in Table 5.

#### 3.1.2.3 SEM Studies

Unless otherwise indicated, scanning electron microscopy was performed on fracture surfaces of fused, heat-treated (crystallized) frit. In the few cases noted, the fused, crystallized glass was reduced to -100 mesh powder (< 150 micron) for examination. In either case (fracture surface or powder), surface preparation consisted of the following steps:

- Acid etch (15 percent by wt. HF/15 percent by wt. HCl in water) followed by water rinse, ammonia neutralization, water rinse, acetone rinse, and air dry on copper mounting block.
- Overcoat with ~ 100 Å of vacuum evaporated carbon followed by 100 Å of evaporated silver.

Examination was made using a Jeolco JSM-2 scanning electron microscope operating with a 25 kv electron beam focused to approximately 100 Å. All pictures were taken using a secondary electron emission mode.

Representative SEM photomicrographs are presented in Figures 4 through 21. These may be correlated with crystallite phases identified in Table 5. It is important to note that although the crystal form for zircon is tetragonal and for zirconia is monoclinic, the shape or habit displayed in

# TABLE 5. CORRELATION OF CRYSTALLIZATION WITH X-RAY DIFFRACTION DATA

| Specimen | Heat Treatment of Frit | | | | | Crystallite Content,[b] wt % | | | | | Glass Content[b] wt % | Crystallite Properties | | |
|---|---|---|---|---|---|---|---|---|---|---|---|---|---|---|
| | Avg. Est. Grain Size (µm) Before Nucleation | Nucleation | | Crystal Growth | | Zircon | Zirconia | β-Spodumene | Silica Phases | $\alpha$-$Al_2O_3$ | | Size (est.), micron | | Uniformity of Distribution |
| | | Time, $10^3$ sec | Temp., °C | Time, $10^3$ sec | Temp., °C | | | | | | | Range | "Avg." | |
| HF-10 | – | – | – | – | – | ND | 5-10 | ND | ND | ND | 90-95 | – | – | – |
| HF-10-A-4 | <37 | 3.6 | 575 | 14.4 | 760 | 25-35 | ND | 50-60[f] | ND | ND | 5-25 | – | – | – |
| HF-10-B-4 | <37 | 3.6 | 575 | 14.4 | 860 | 20-30 | ND | 35-50[f] | ND | ND | 20-45 | – | – | – |
| HF-10-C-4 | <37 | 3.6 | 575 | 14.4 | 960 | 22-32 | ND | 50-60[f] | ND | ND | 8-28 | – | – | – |
| HF-10-D-4 | <37 | 3.6 | 575 | 14.4 | 1130 | 25-35 | ND | 45-55[f] | ND | ND | 10-30 | – | – | – |
| HF-17 | – | – | – | – | – | ND | >7 | ND | ND | ND | 93-100 | – | – | – |
| HF-17-A-4 | <37 | 3.6 | 575 | 14.4 | 760 | 25-35[b] | ND | 40-50[f] | ND | ND | 15-35 | – | – | – |
| HF-17-B-4 | <37 | 3.6 | 520 | 14.4 | 860 | 15-25 | ND | 20-30 | ND | ND | 45-65 | – | – | – |
| HF-17-C-0.5[a] | <37 | 3.6 | 550 | 1.8 | 960 | 15-20 | 5-10 | ND | ND | ND | 70-80 | 0.2-4 | 1-2 | Fair |
| HF-17-C-1[a] | <37 | 3.6 | 550 | 3.6 | 960 | 15-20 | 5-10 | ND | ND | ND | 70-80 | 0.2-4 | 1-2 | Poor |
| HF-17-C-3 | <37 | 3.6 | 550 | {3.6 at<br>{7.2 at | 920<br>1005 | 15-25 | ~5 | ND | ND | ND | 70-80 | 1-2 | 1-2 | Poor |
| HF-17-C-4 | <37 | 3.6 | 575 | 14.4 | 960 | 15-30 | >10 | >10 | ND | ND | <50-65 | 1-2 | 1-2 | Poor |
| HF-17-C-8 | <37 | 3.6 | 550 | {3.6 at<br>{25 at | 920<br>1005 | 15-25 | ~5 | ND | ND | ND | 70-80 | – | – | – |
| HF-18 | – | – | – | – | – | ND | ~10 | ND | ND | ND | 90 | – | – | – |
| HF-18[a] | – | – | – | – | – | ND | ~10 | >5 | ND | ~5 | 80 | – | – | – |
| HF-18-4[a] | <37 | 1.8 | 500 | 1.8 | 960 | ND | 30 | ND | 40 $\alpha$-cristobalite<br>10 o-silica | ND | ~20 | – | – | – |
| HF-18-5[a] | <37 | 1.8 | 550 | 1.8 | 925 | ND | 30 | ND | 10-20 $\alpha$-cristobalite<br>50 o-silica | ND | <10 | – | – | – |
| HF-18-6[a] | <37 | 1.8 | 550 | 1.8 | 960 | ND | 30 | ND | 5-10 $\alpha$-cristobalite<br>35 o-silica | <5 | 20-25 | – | – | – |
| HF-18-7[a] | <37 | 1.8 | 550 | 1.8 | 1100 | 15-25 | >20 | ND | ND | >5 | <50-60 | – | – | – |

(Table 5, continued)

| Specimen | Heat Treatment of Frit | | | | | Crystallite Content,[b] wt % | | | | | Glass Content,[b] wt % | Crystallite Properties | | |
|---|---|---|---|---|---|---|---|---|---|---|---|---|---|---|
| | Avg. Est. Grain Size (μm) Before Nucleation | Nucleation | | Crystal Growth | | Zircon | Zirconia | β-Spodumene | Silica Phases | $\alpha$-$Al_2O_3$ | | Size (est.), micron | | Uniformity of Distribution |
| | | Time, $10^3$ sec | Temp., °C | Time, $10^3$ sec | Temp., °C | | | | | | | Range | "Avg." | |
| HF-20 | -- | – | – | – | – | ND | >3 | ND | ND | ND | <97 | – | – | – |
| HF-20-A-4 | <37 | 3.6 | 550 | 14.4 | 800 | 25 | ND | 15 | 10 o-silica | ND | 50 | – | – | – |
| HF-20-B-4 | <37 | 3.6 | 550 | 14.4 | 900 | 25-35 | >3 | ND | ND | ND | 62-72 | – | – | – |
| HF-20-C-3 | <37 | 3.6 | 550 | {3.6 at<br>{7.2 at | 920<br>1005 | 20-35 | ND | ND | >10 $\alpha$-quartz | ND | 55-70 | – | – | – |
| HF-20-C-4 | <37 | 3.6 | 550 | 14.4 | 960 | 15-25 | ND | ND | 25-35 $\alpha$-quartz<br>>5 $\alpha$-cristobalite | ND | 35-55 | 0.3-4 | 1-2 | Poor |
| HF-20-C-8 | <37 | 3.6 | 550 | {3.6 at<br>{25 at | 920<br>1005 | 25-35 | >5 | ND | ND | ND | 60-70 | – | – | – |
| HF-20-D-4 | <37 | 3.6 | 550 | 14.4 | 1125 | 20-30 | ND | ND | ND | ND | 70-80 | – | – | – |
| HF-20-1[a] | <37 | 1.8 | 500 | 1.8 | 900 | 35 | ND | ND | 15 o-silica<br>>10 $\alpha$-cristobalite | ND | <40 | – | – | – |
| HF-20-3[a] | <37 | 1.8 | 550 | 1.8 | 900 | 30 | ND | 25 | 25 o-silica | ND | 20 | 0.3-4 | 1-2 | Poor |
| HF-21-1[a] | <37 | 1.8 | 500 | 1.8 | 900 | 25-30 | ND | 25 | 25 o-silica | ND | <25 | – | – | – |
| HF-21-3[a] | <37 | 1.8 | 550 | 1.8 | 900 | 25-30 | ND | 30 | 25 o-silica | ND | <25 | – | – | – |
| HF-22 | <37 | – | – | – | – | ND | >5 | ND | ND | ND | <95 | – | – | – |
| HF-23 | – | – | – | – | – | ND | ND | ND | ND | ND | 100 | – | – | – |
| HF-23-1[a] | <37 | 1.8 | 550 | 1.8 | 960 | 25-35 | ND | 25-35 | >10 $\alpha$-quartz<br>>5 $\alpha$-cristobalite | ND | 15-35 | – | – | – |
| HF-24 | – | – | – | – | – | ND | ND | ND | ND | ND | 100 | – | – | – |
| HF-24-1 | 884-1680 | 1.8 | 500 | 1.8 | 900 | 7 | ND | ND | ND | ND | 93 | 0.2-2 | 1-2 | Very poor[e] |
| HF-24-8 | <125 | 1.8 | 500 | 1.8 | 900 | ~10 | ND | ND | ND | ND | ~90 | 0.5-4 | 2 | Poor |
| HF-24-10 | <125 | 1.8 | 550 | 1.8 | 900 | 10-15 | ND | ND | ND | ND | 85-90 | – | – | – |
| HF-24-11 | <44 | 1.8 | 550 | 1.8 | 900 | 10-15 | ND | ND | ND | ND | 85-90 | 0.5-3 | 1-2 | Fair |
| HF-24-PX | 1-40 | 1.8 | 500 | 1.8 | 900 | 10-15 | ND | ND | ND | ND | 85-90 | 0.2-0.8 | 0.5 | Good |

(Table 5, continued)

| Specimen | Heat Treatment of Frit | | | | | Crystallite Content,[b] wt % | | | | | Glass Content[b] wt % | Crystallite Properties | | |
|---|---|---|---|---|---|---|---|---|---|---|---|---|---|---|
| | Avg. Est. Grain Size (μm) Before Nucleation | Nucleation | | Crystal Growth | | Zircon | Zirconia | β-Spodumene | Silica Phases | $\alpha$-$Al_2O_3$ | | Size (est.) micron | | Uniformity of Distribution |
| | | Time, $10^3$ sec | Temp., °C | Time, $10^3$ sec | Temp., °C | | | | | | | Range | "Avg." | |
| HF-40-2 | 150 | 1.8 | 500 | 1.8 | 880-910 | 3 | ND | ND | ND | ND | 97 | – | – | – |
| HF-41-2 | 150 | 1.8 | 500 | 1.8 | 880-910 | 5-10 | ND | ND | ND | ND | 90-95 | – | – | – |
| HF-42-2 | 150 | 1.8 | 500 | 1.8 | 880-910 | 15-20 | ND | ND | ND | ND | 80-85 | – | – | – |
| HF-43-2 | 150 | 1.8 | 500 | 1.8 | 880-910 | 10-15 | ND | ND | ND | ND | 85-90 | – | – | – |
| HF-44-2 | 150 | 1.8 | 500 | 1.8 | 875-900 | 11 | ND | ND | ND | ND | 89 | – | – | – |
| HF-45-1 | <100 | 3.0 | 500 | 1.8 | 890-920 | 25 | ND | ND | ND | ND | 75 | 0.2-4 | 1-3 | Fair |
| HF-52-PX | 1-40 | 1.8 | 500 | 1.8 | 900 | 15 | 15 | ND | ND | ND | 70 | 0.1-3 | 0.3-0.7 | Good |
| HF-53-PX | 1-40 | 1.8 | 500 | 1.8 | 900 | <1 | 25 | ND | ND | ND | ~75 | 0.1-6 | 0.5 | Good |

[a] HCl-washed, water-rinsed, and dried prior to nucleation and crystallization.
[b] Estimated from X-ray diffraction spectra. Glass content obtained by difference. In certain cases, zircon contents are greater than theoretical, indicating a silica-rich or excess silica phase.
[c] Includes minor amounts of one or more unidentified phases.
[d] Almost entirely large dendrites. See Figure 18.
[e] Clustered badly with some unidentified skeletal-type structure
[f] Believed high by virtue of being silica-rich.

(Table 5, continued)

| Specimen | Heat Treatment of Frit | | | | | Crystallite Content,[b] wt % | | | | | Glass Content[b] wt % | Crystallite Properties | | |
|---|---|---|---|---|---|---|---|---|---|---|---|---|---|---|
| | Avg. Est. Grain Size (μm) Before Nucleation | Nucleation | | Crystal Growth | | Zircon | Zirconia | β-Spodumene | Silica Phases | $\alpha$-$Al_2O_3$ | | Size (est.) micron | | Uniformity of Distribution |
| | | Time, $10^3$ sec | Temp., °C | Time, $10^3$ sec | Temp., °C | | | | | | | Range | "Avg." | |
| HF-25 | – | – | – | – | – | ND | ND | ND | ND | ND | 100 | – | – | – |
| HF-25-1 | 884-1680 | 1.8 | 500 | 1.8 | 900 | <1 | ND | ND | ND | ND | >99 | – | – | – |
| HF-26 | – | – | – | – | – | ND | ND | ND | ND | ND | 100 | – | – | – |
| HF-26-1 | 884-1680 | 1.8 | 500 | 1.8 | 900 | 7 | ~1 | ND | ND | ND | ~92 | 0.3-2 | 0.8-1 | Very poor |
| HF-26-3 | <125 | 1.8 | 500 | 1.8 | 900 | 10-15 | ND | ND | ND | ND | 85-90 | 0.5-5 | 2 | Poor |
| HF-26-5 | <125 | 1.8 | 550 | 1.8 | 900 | ~10 | ND | ND | ND | ND | ~90 | 0.3-3 | 2 | Poor |
| HF-27 | – | – | – | – | – | ND | ND | ND | ND | ND | 100 | – | – | – |
| HF-27-1 | 884-1680 | 1.8 | 500 | 1.8 | 900 | ~5 | ND | ND | ND | ND | ~95 | – | – | – |
| HF-28 | – | – | – | – | – | ND | ND | ND | ND | ND | 100 | – | – | – |
| HF-28-1 | 884-1680 | 1.8 | 500 | 1.8 | 900 | ~8 | ND | ND | 1-5 $\alpha$-cristobalite | ND | 87-91 | – | – | – |
| HF-28-3 | <125 | 1.8 | 500 | 1.8 | 900 | ~15 | ND | ND | 5-10 $\alpha$-cristobalite | ND | 75-80 | 0.5-2 | 1 | Fair |
| HF-28-5 | <125 | 1.8 | 550 | 1.8 | 900 | ~15 | ND | ND | 5-10 $\alpha$-cristobalite | ND | 75-80 | – | – | – |
| HF-28-PX | 1-40 | 1.8 | 500 | 1.8 | 900 | 15-25 | ND | ND | ND | ND | 75-85 | 0.2-1 | 0.5 | Good |
| HF-34-1 | Bulk | – | – | 3.6 | 875-925 | ND | ND | ND | 10 $TiO_2:ZrO_2$ | ND | 90 | – | – | – |
| HF-34-2 | 1-40 | 1.8 | 500 | 5.4 | 900 | 5-10 | ND | <10 | 5-10 $TiO_2:ZrO_2$ | 10 | >60-70 | – | – | – |
| HF-35-2 | 1-40 | 1.8 | 500 | 3.6 | 900-925 | 10-15 | ND | ~5 | ND | ND | 70-80[c] | – | – | – |
| HF-39-1 | Bulk | – | – | 4.2 | 875-925 | ND | 5 | ND | ND | ND | 95 | – | – | d |
| HF-39-2 | 1-40 | 3.6 | 50 | 1.8 | 900 | ~10 | – | ~10 | <5 $\alpha$-quartz<br><5 β-eucryptite | ND | ~70[c] | – | – | – |

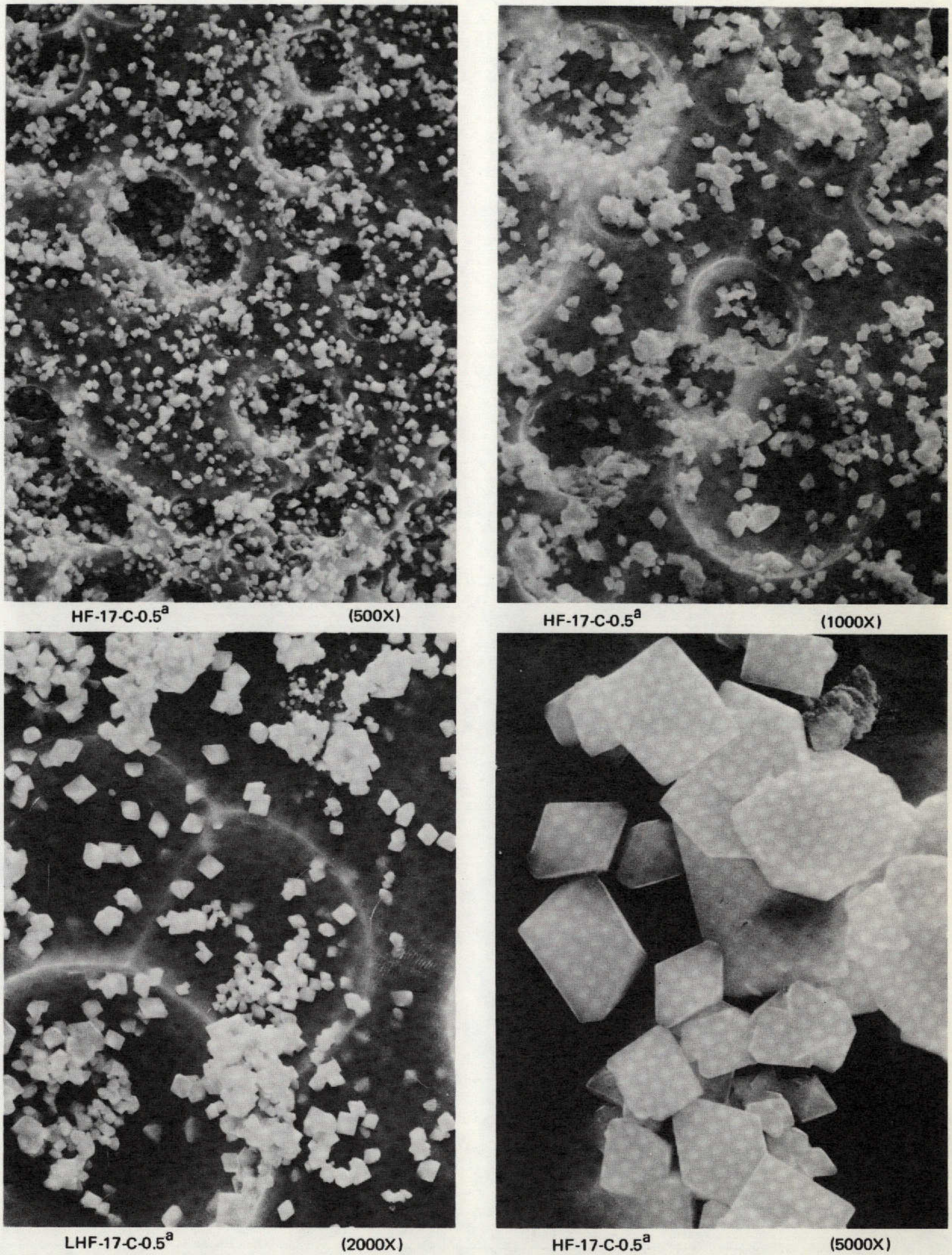


Figure 4. Scanning electron photomicrographs of crystallized frit HF-17-C-0.5[a] (footnote a — see Table 5)

This page is reproduced at the back of the report by a different reproduction method to provide better detail.

This page is reproduced at the back of the report by a different reproduction method to provide better detail.

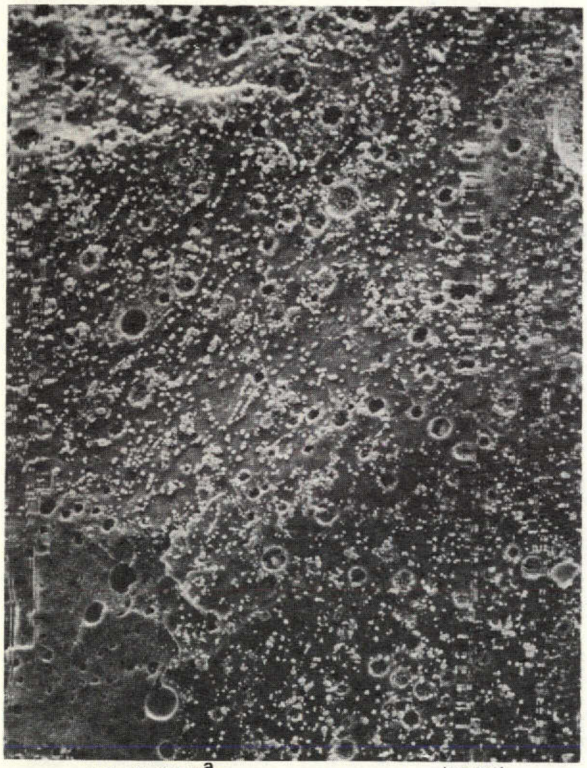

HF-17-C-1.0[a] (100X)

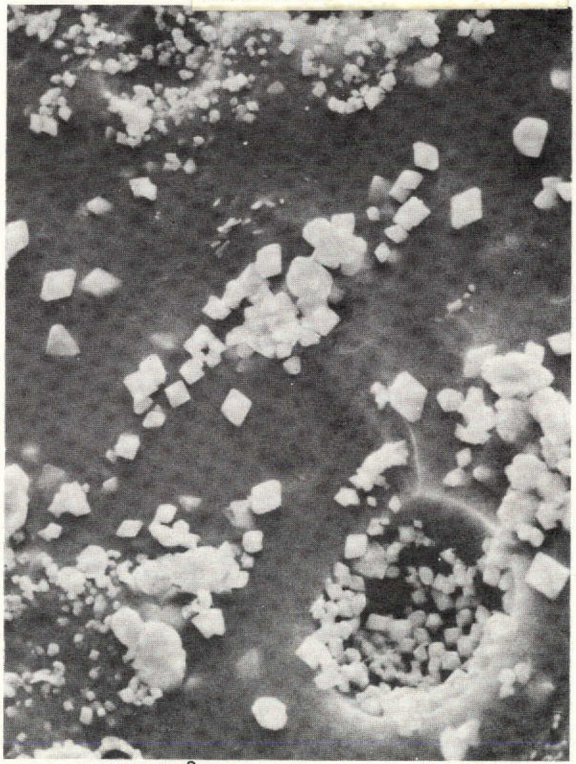

HF-17-C-1.0[a] (1000X)

Figure 5. Scanning electron photomicrographs of crystallized frit HF-17-C-1.0[a] (footnote a — see Table 5)

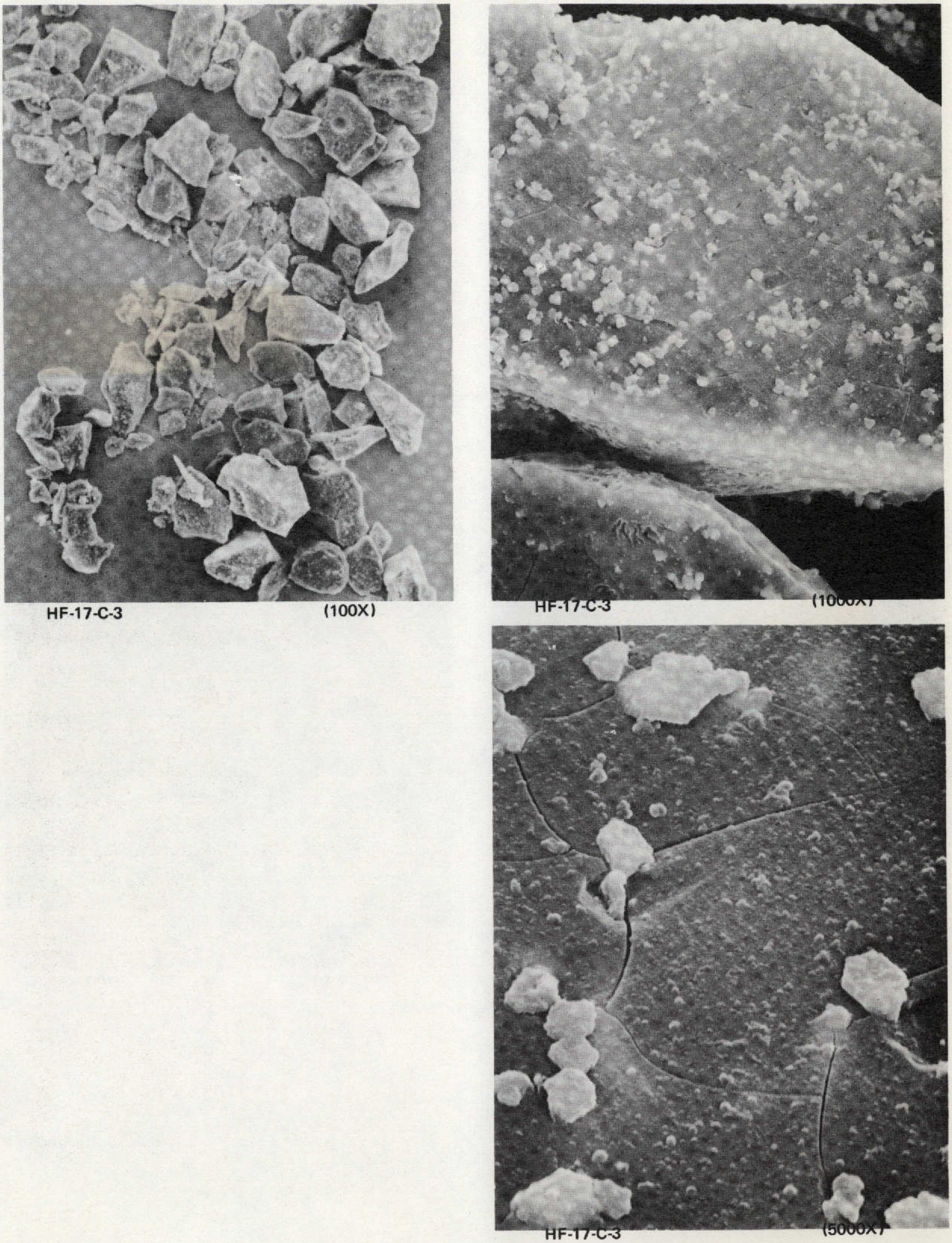


Figure 6. Scanning electron photomicrographs of crystallized frit HF-17-C-3 (powder specimen)

This page is reproduced at the back of the report by a different reproduction method to provide better detail.

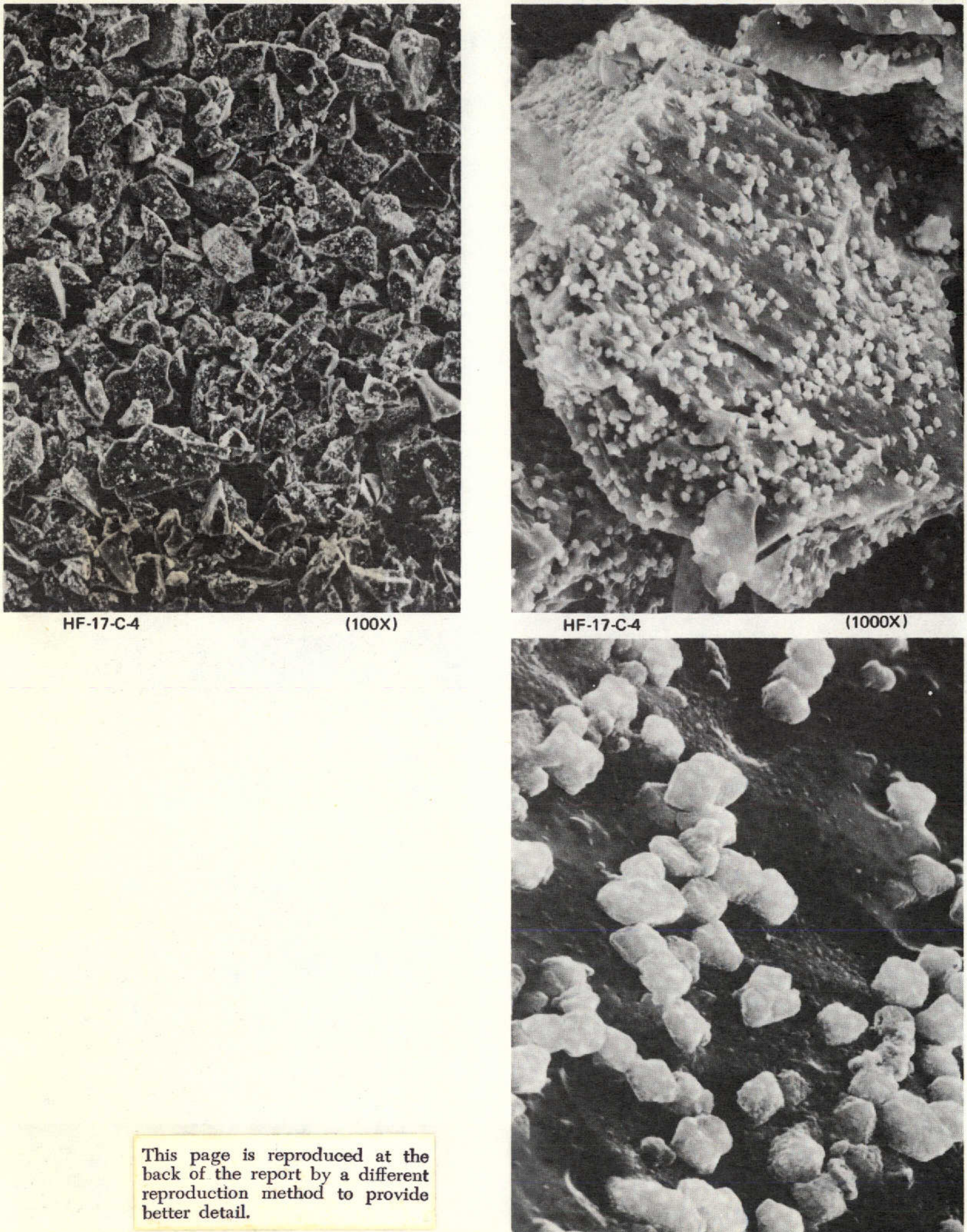

HF-17-C-4 (100X)

HF-17-C-4 (1000X)

HF-17-C-4 (5000X)

This page is reproduced at the back of the report by a different reproduction method to provide better detail.

Figure 7. Scanning electron photomicrographs of crystallized frit HF-17-C-4 (powder specimen)

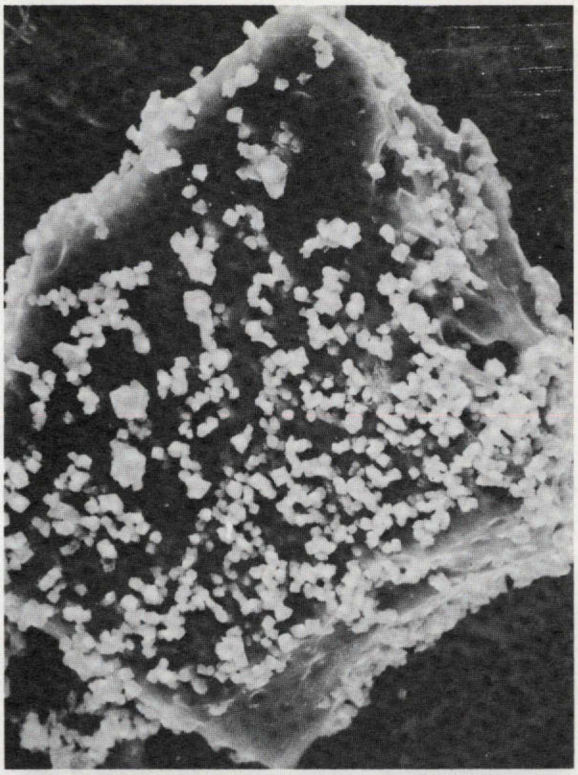

HF-20-C-4 (1000X)

This page is reproduced at the back of the report by a different reproduction method to provide better detail.

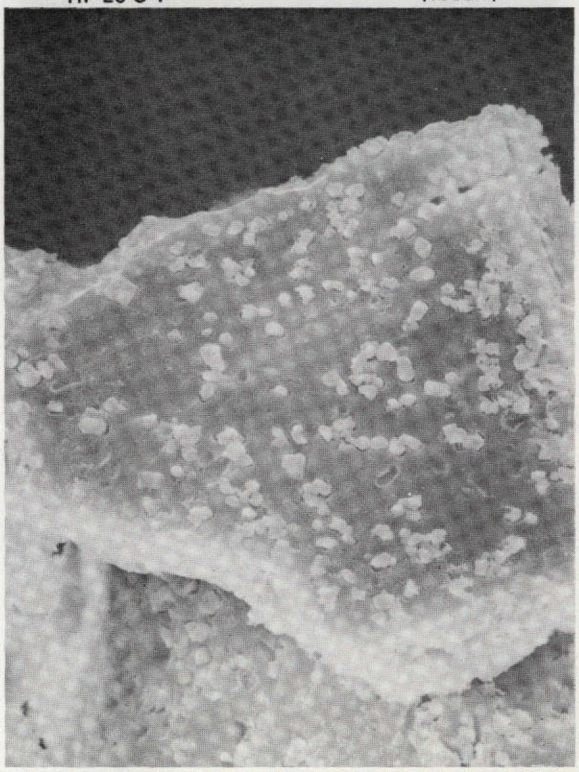

HF-20-3[a] (1000X)

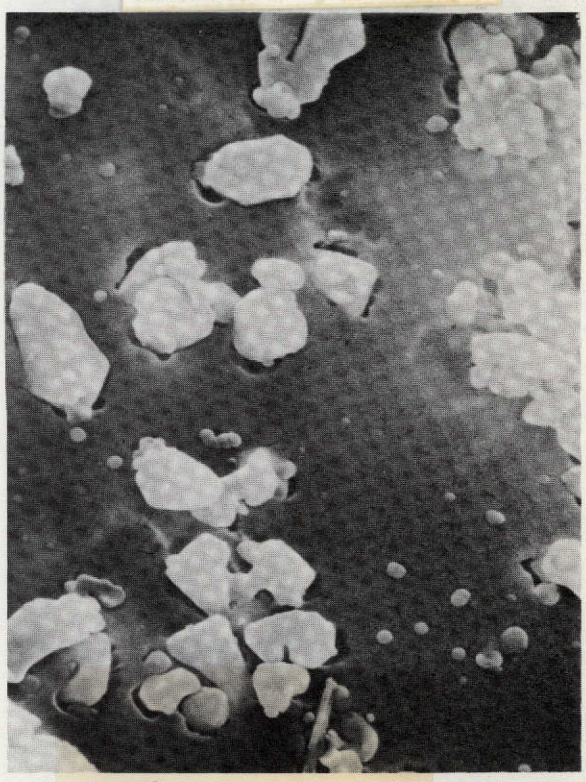

HF-20-3[a] (5000X)

Figure 8. Scanning electron photomicrographs of crystallized frits HF-20-C-4 and -20-3 (powder specimens)

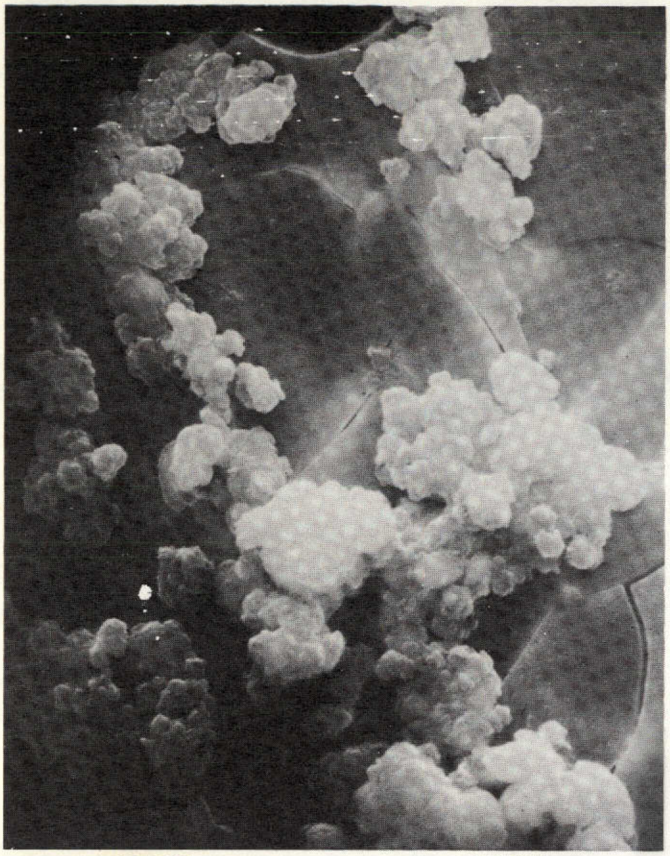

HF-24-1 (5000X)

This page is reproduced at the back of the report by a different reproduction method to provide better detail.

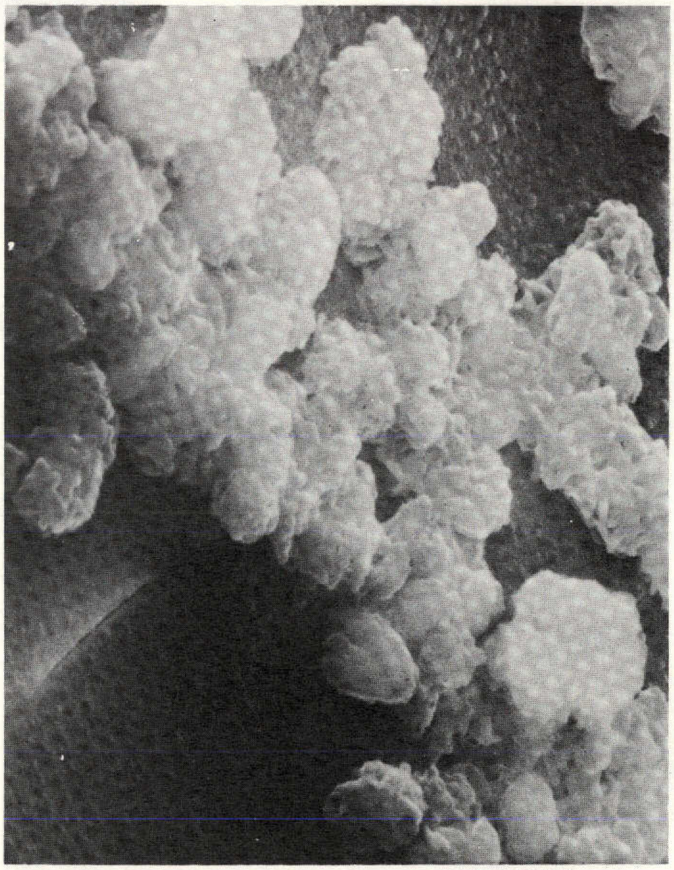

HF-24-1 (10,000X)

Figure 9. Scanning electron photomicrographs of crystallized frit HF-24-1

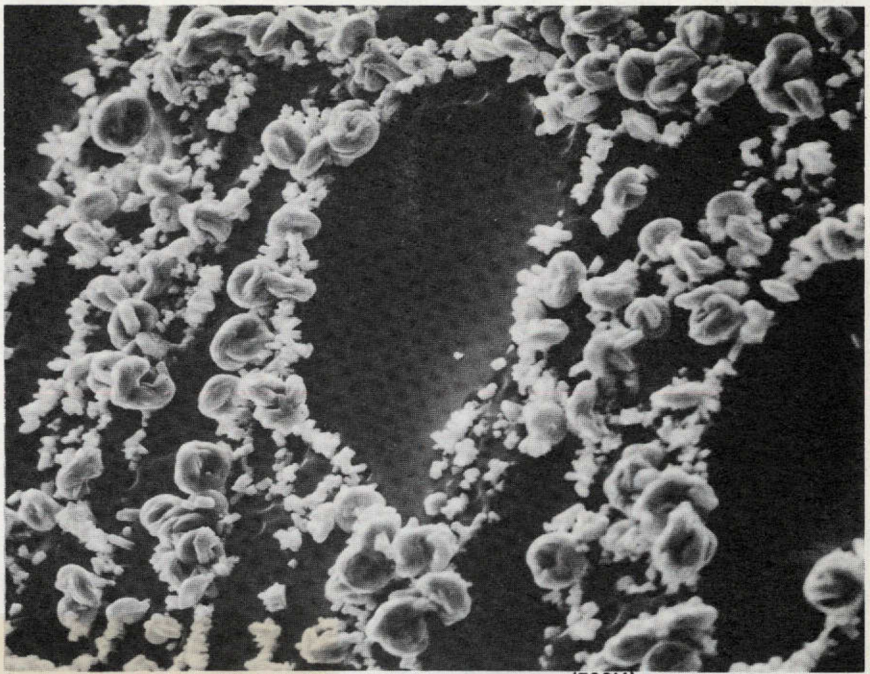

HF-24-8 (A) (500X)

HF-24-8 (A) (5000X)

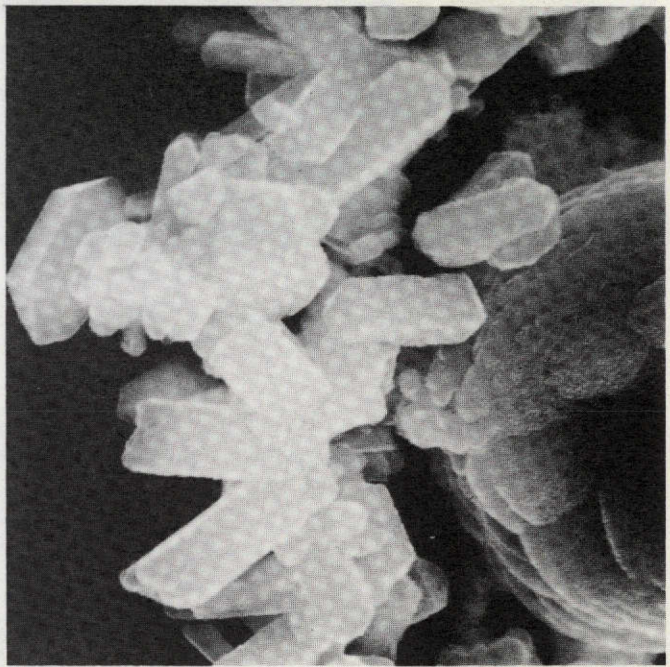

HF-24-8 (A) (5000X)

Figure 10. Scanning electron photomicrographs of crystallized frit HF-24-8 (specimen A)



This page is reproduced at the back of the report by a different reproduction method to provide better detail.

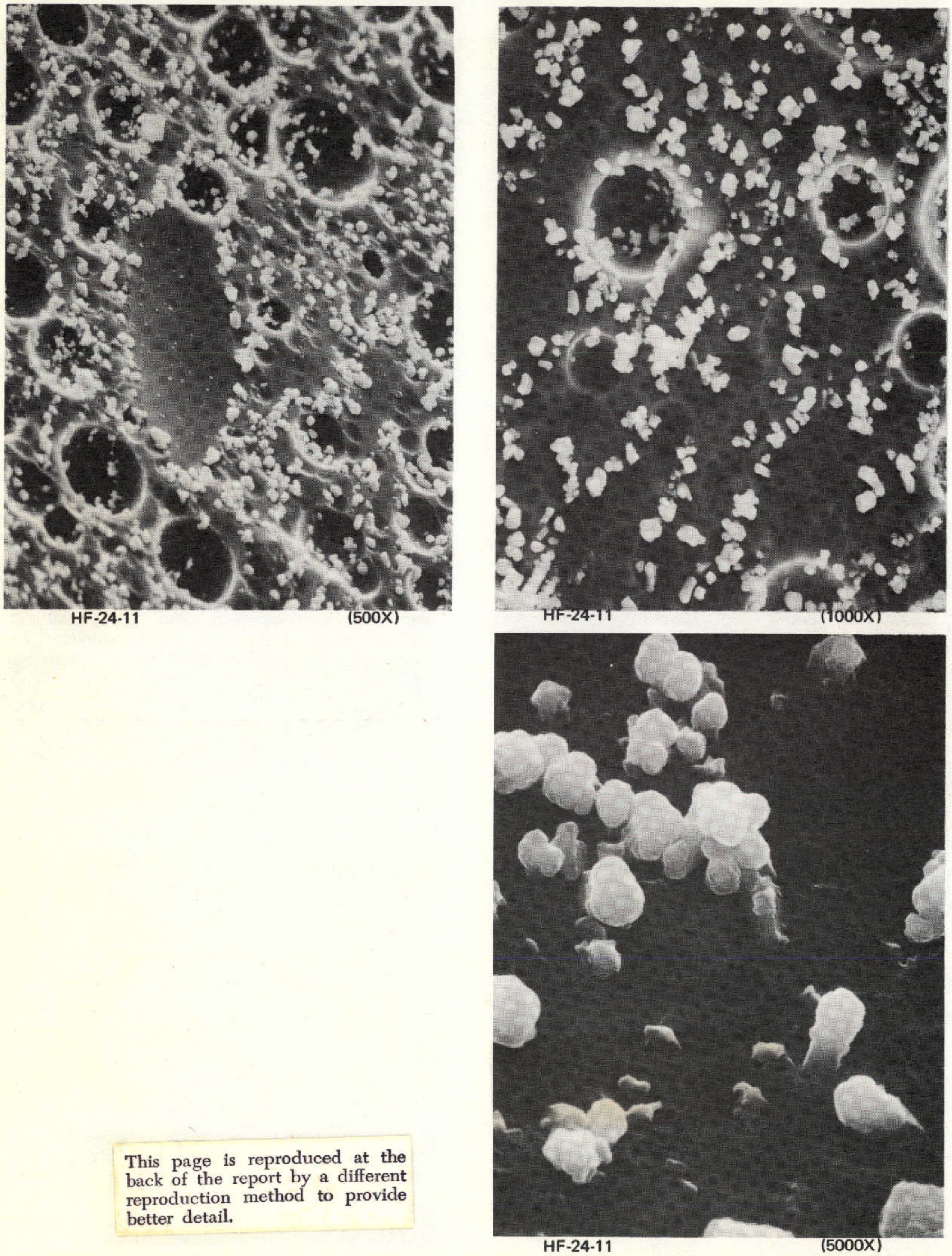


This page is reproduced at the back of the report by a different reproduction method to provide better detail.

Figure 11. Scanning electron photomicrographs of crystallized frit HF-24-11

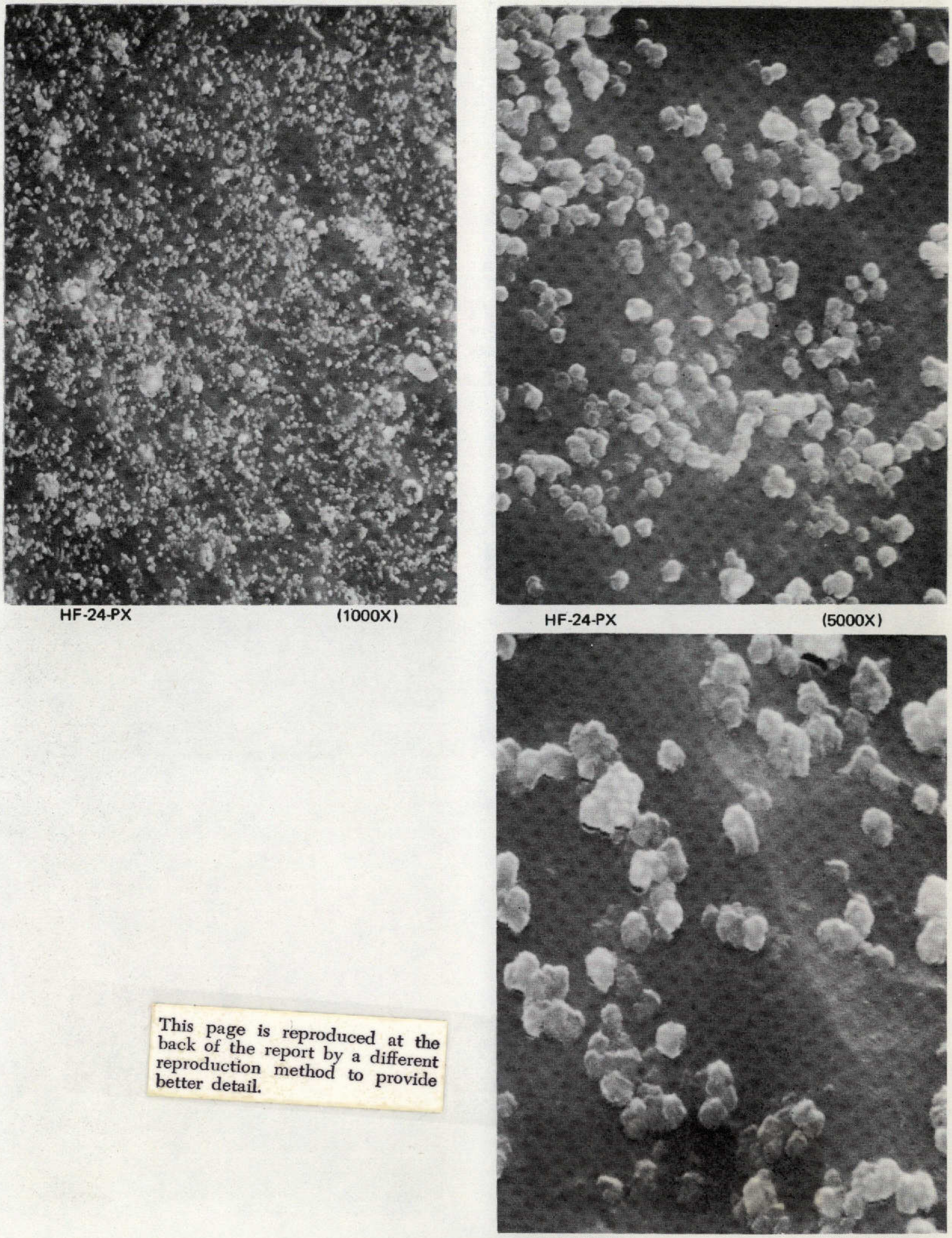

HF-24-PX (1000X)

HF-24-PX (5000X)

HF-24-PX (10,000X)

This page is reproduced at the back of the report by a different reproduction method to provide better detail.

Figure 12. Scanning electron photomicrographs of crystallized frit HF-24-PX

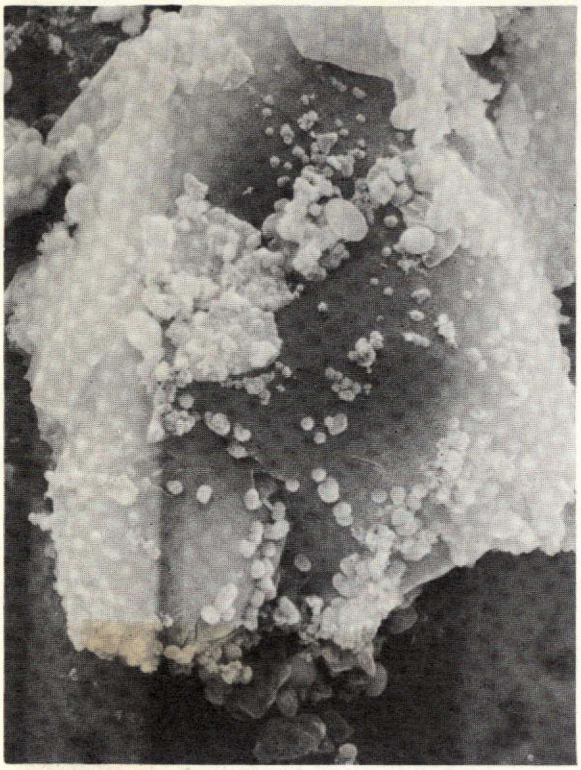

HF-26-1 (3000X)

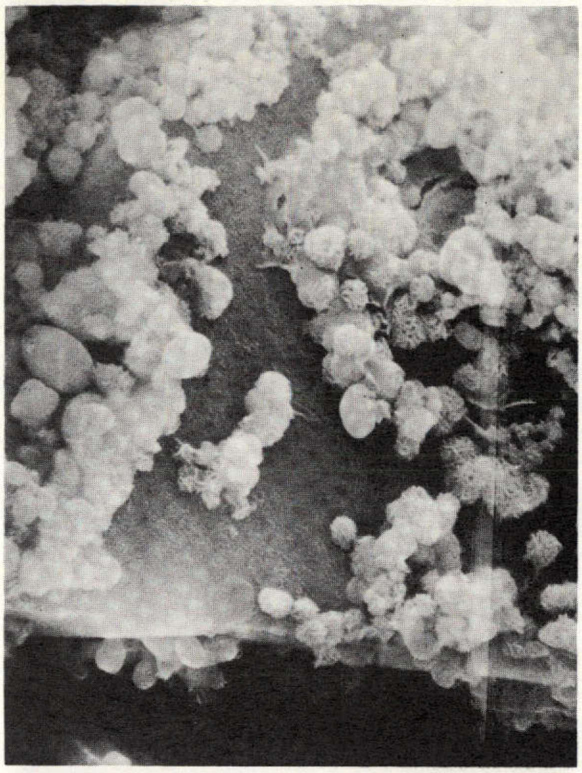

HF-26-1 (5000X)

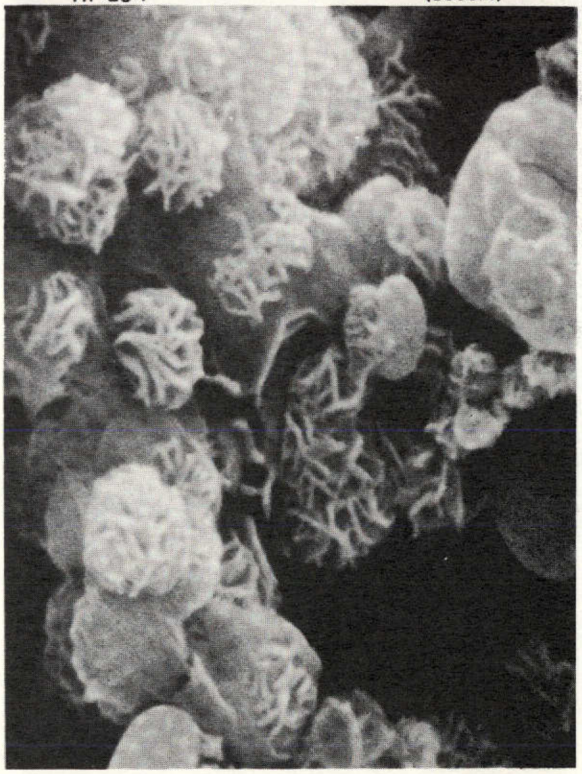

HF-26-1 (20,000X)

This page is reproduced at the back of the report by a different reproduction method to provide better detail.

Figure 13. Scanning electron photomicrographs of crystallized frit HF-26-1

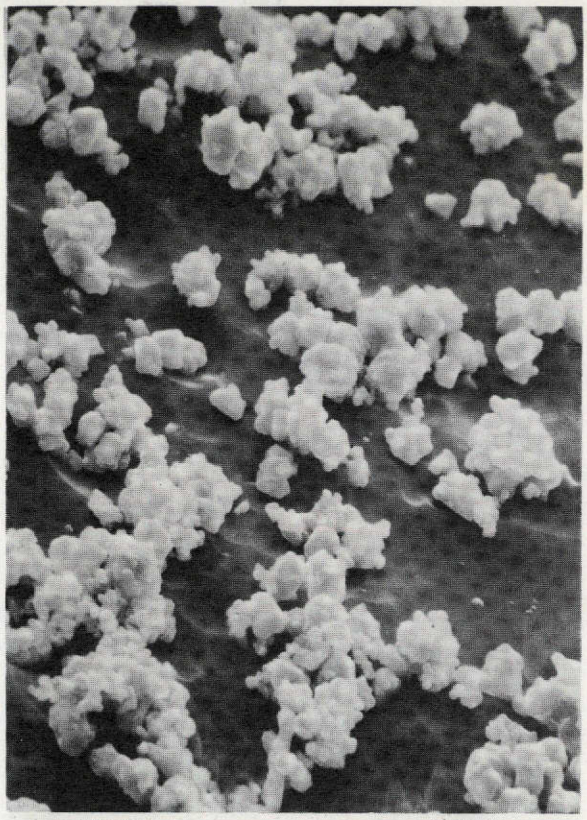

HF-26-3 (1000X)

This page is reproduced at the back of the report by a different reproduction method to provide better detail.

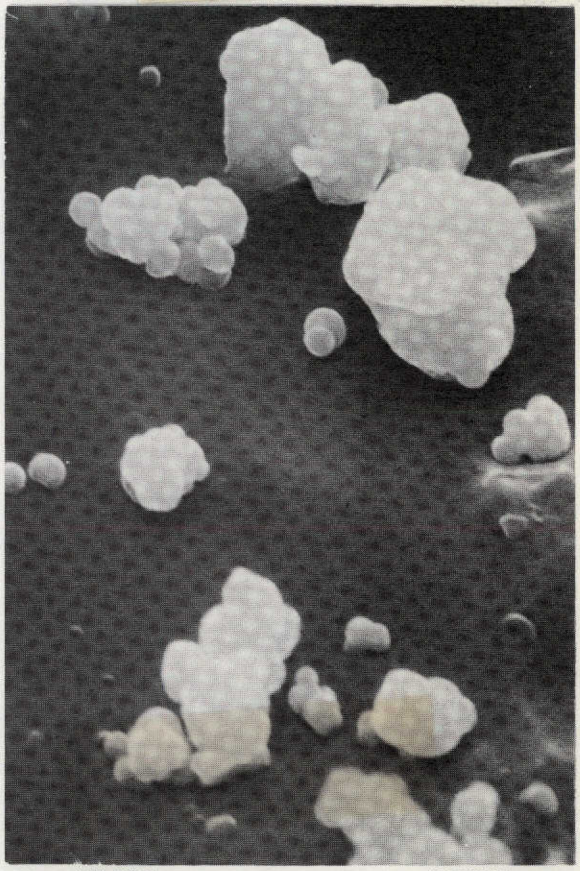

HF-26-3 (5000X)

Figure 14. Scanning electron photomicrographs of crystallized frit HF-26-3

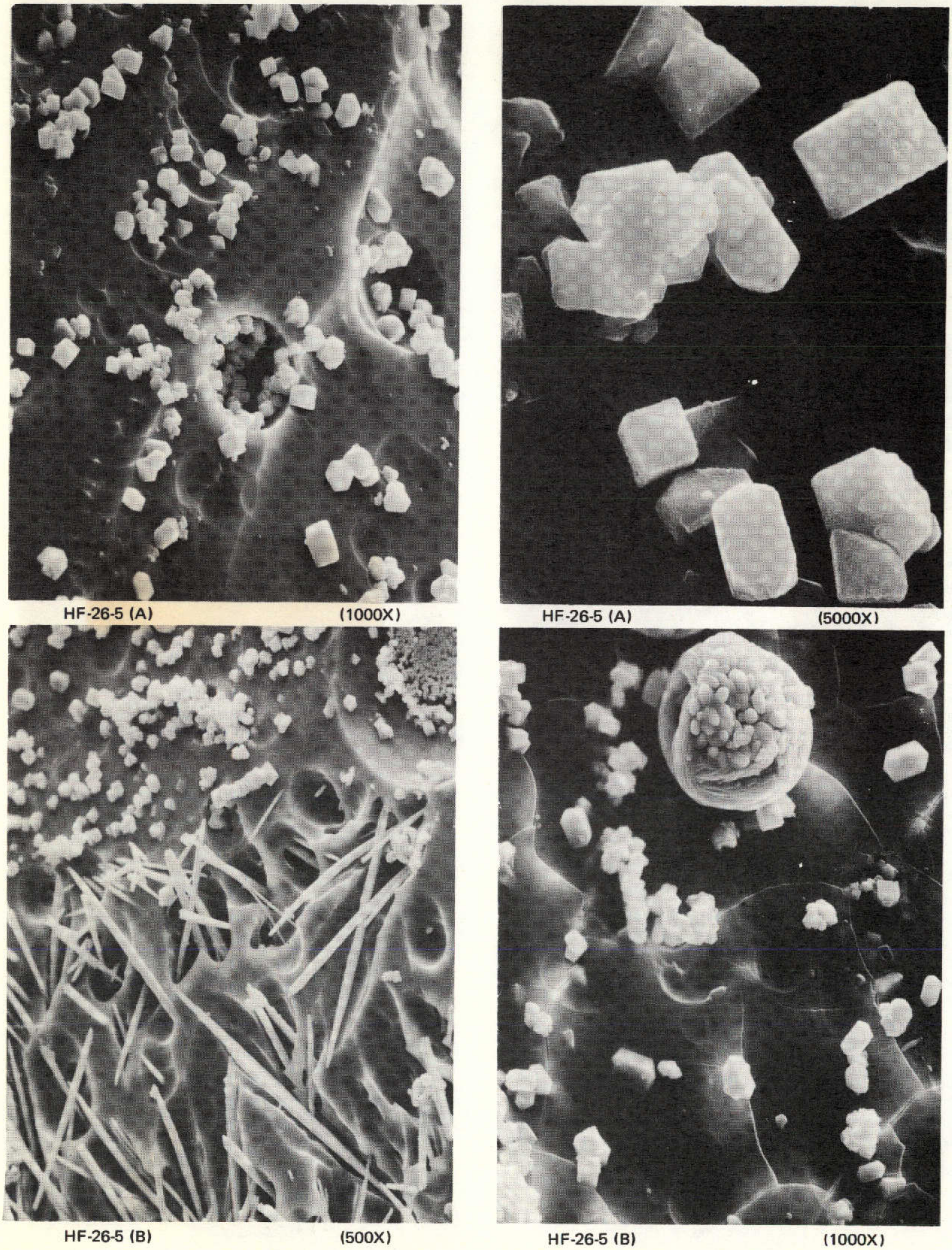


Figure 15. Scanning electron photomicrographs of crystallized frit HF-26-5 (specimens A and B)

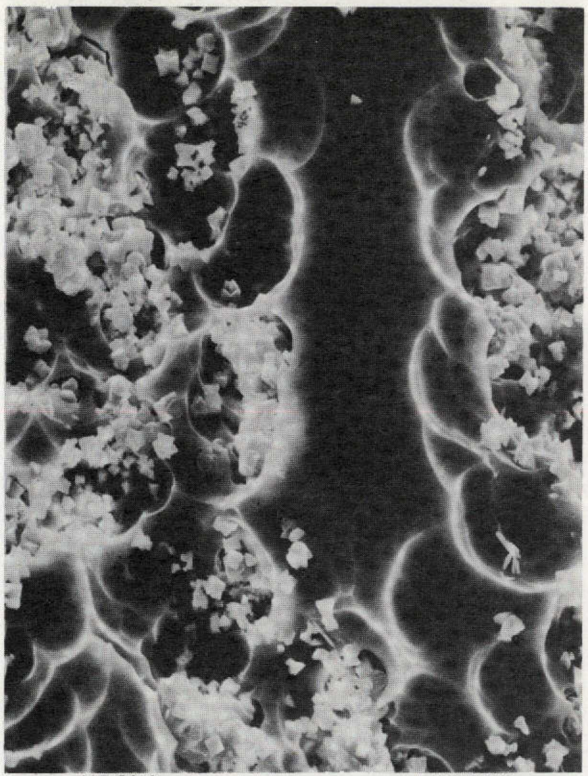

HF-28-3 (1000X)

This page is reproduced at the back of the report by a different reproduction method to provide better detail.

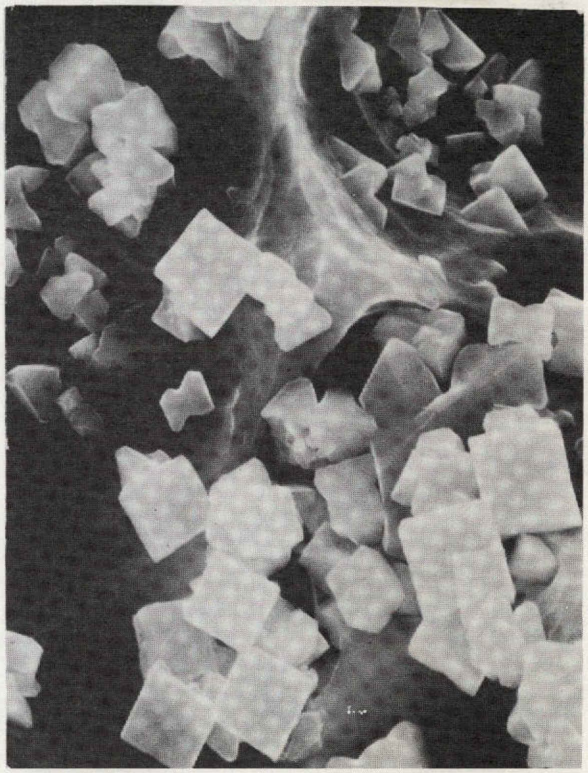

HF-28-3 (5000X)

Figure 16. Scanning electron photomicrographs of crystallized frit HF-28-3

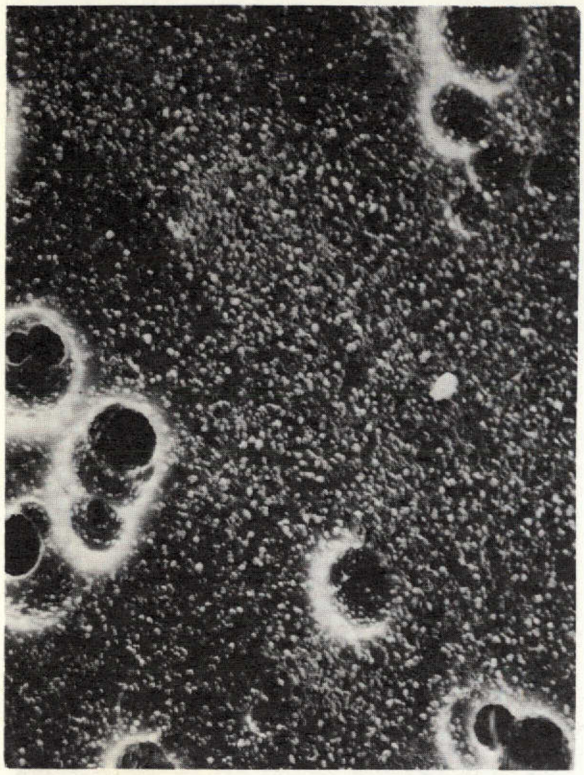

HF-28-PX (1000X)

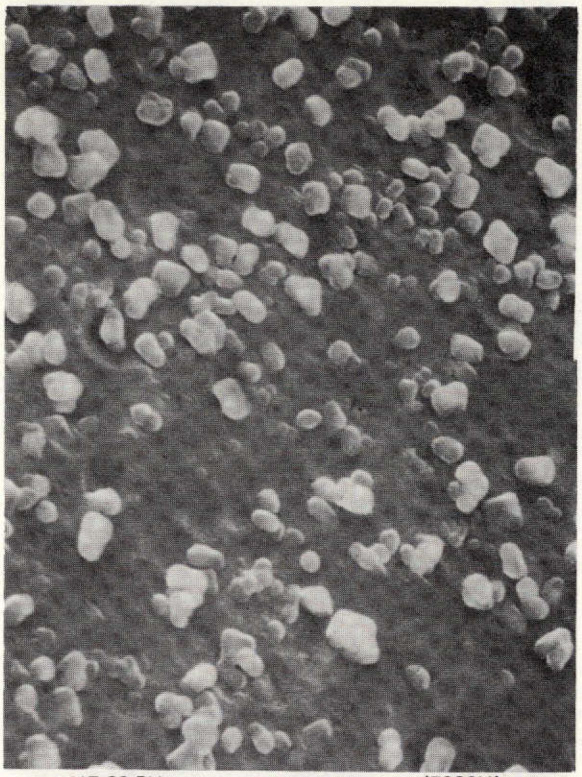

HF-28-PX (5000X)

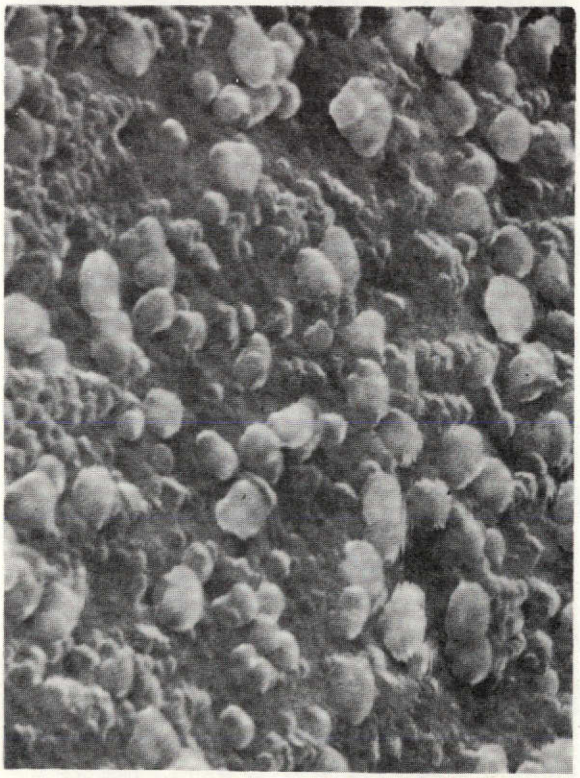

HF-28-PX (10,000X)

This page is reproduced at the back of the report by a different reproduction method to provide better detail.

Figure 17. Scanning electron photomicrographs of crystallized frit HF-28-PX

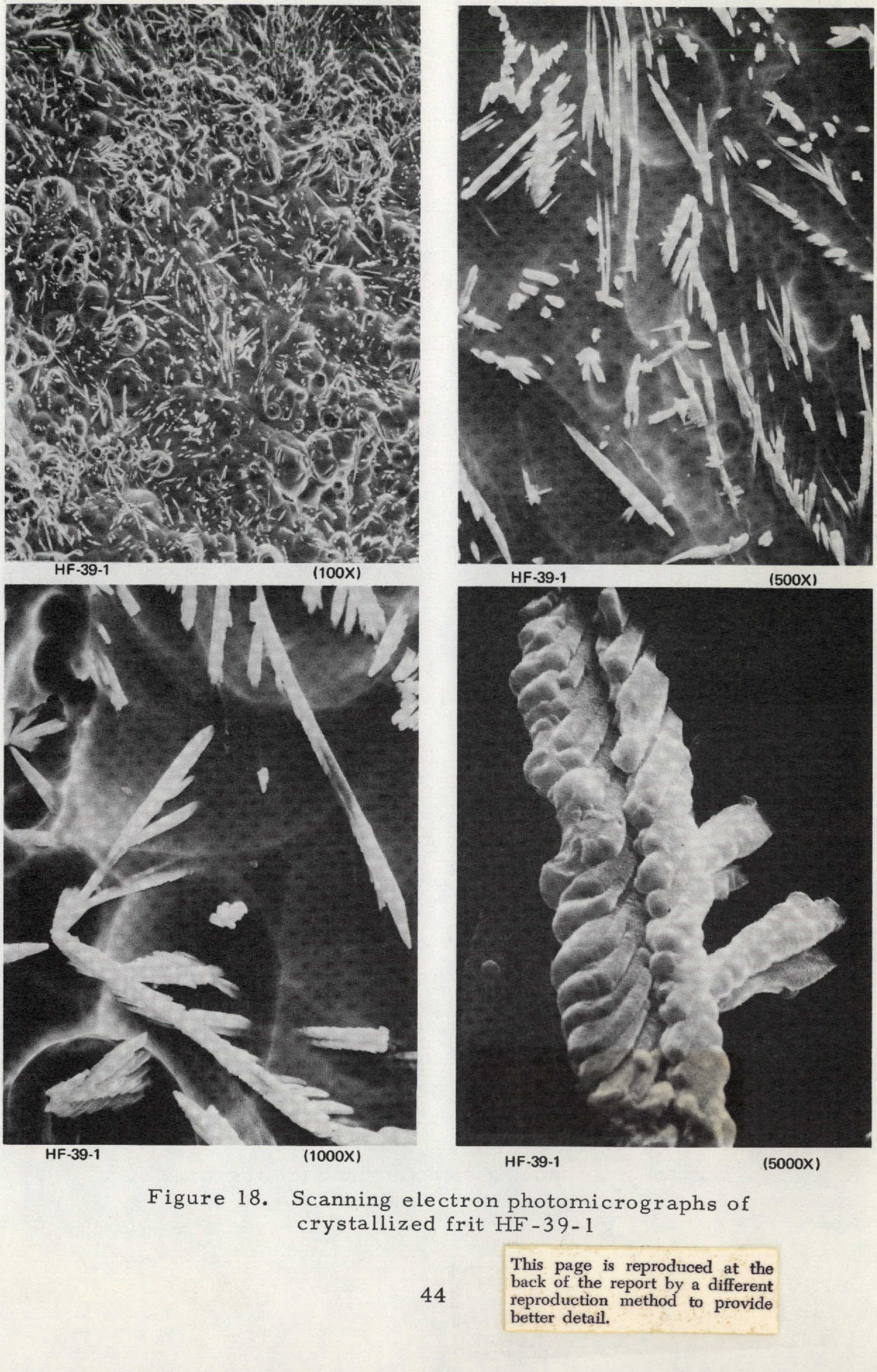


Figure 18. Scanning electron photomicrographs of crystallized frit HF-39-1

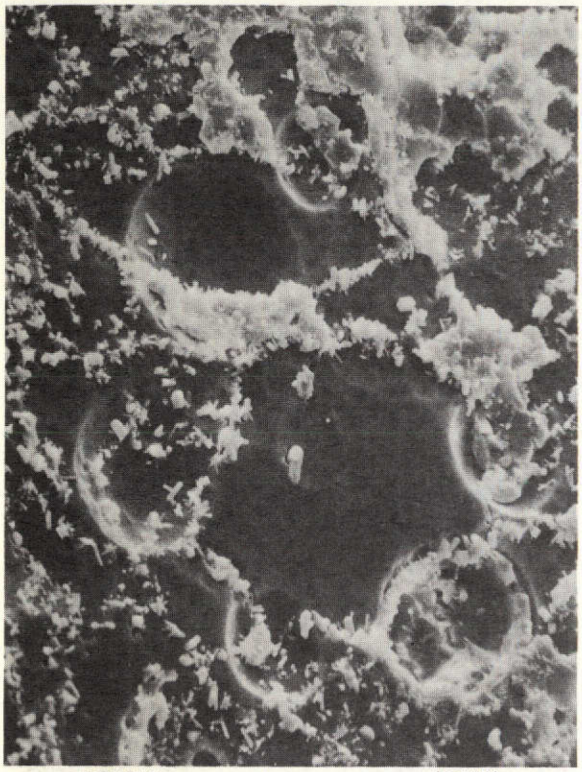

HF-45-1 (500X)

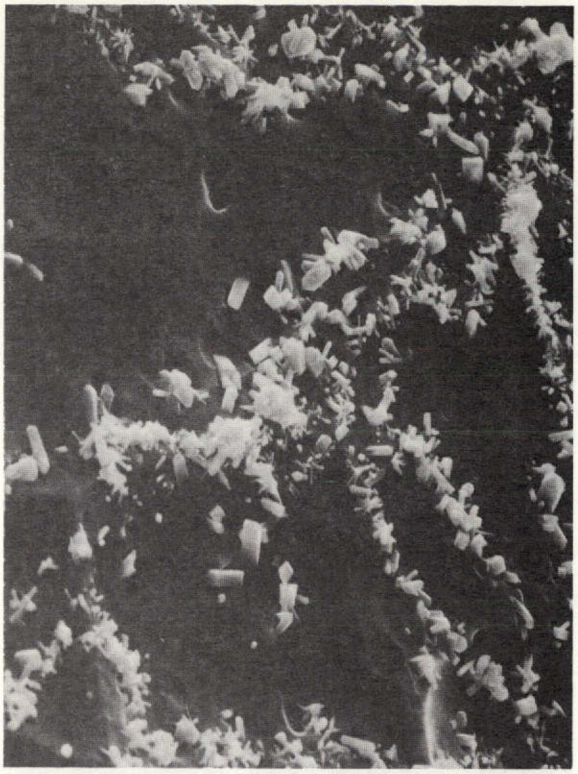

HF-45-1 (1000X)

HF-45-1 (5000X)

This page is reproduced at the back of the report by a different reproduction method to provide better detail.

Figure 19. Scanning electron photomicrographs of crystallized frit HF-45-1

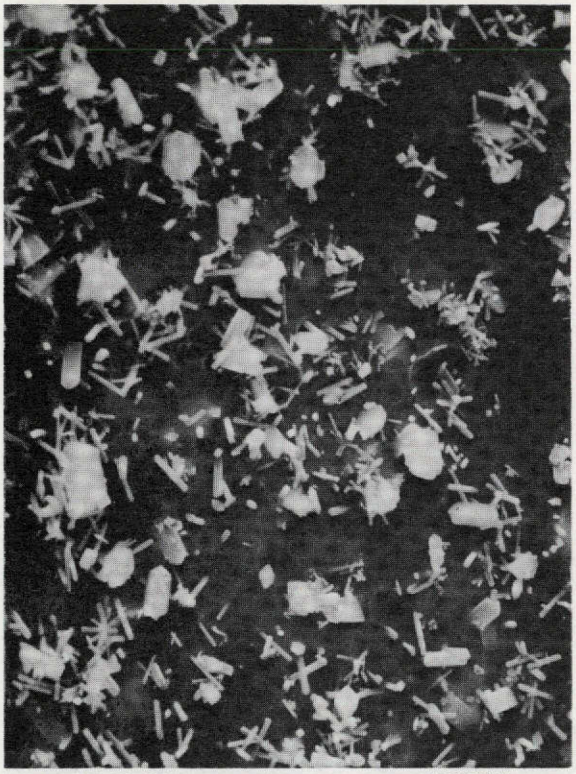

HF-52-PX (3000X)

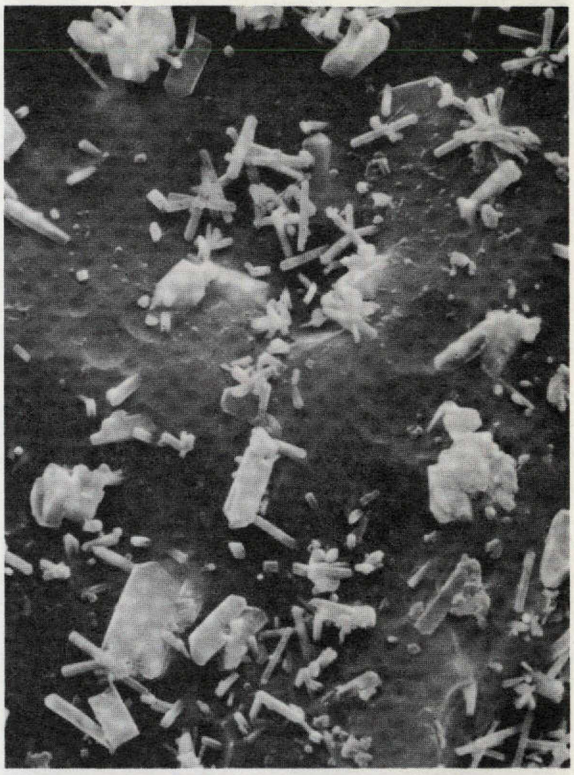

HF-52-PX (5000X)

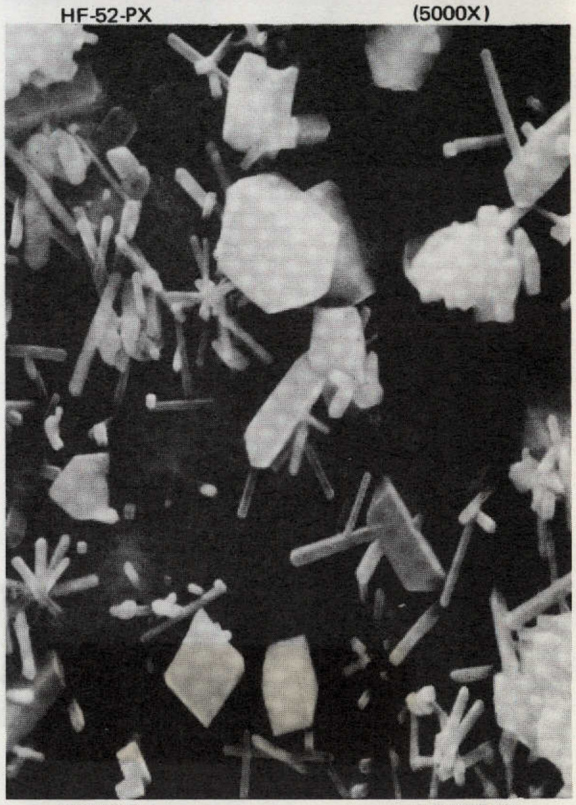

This page is reproduced at the back of the report by a different reproduction method to provide better detail.

HF-52-PX (10,000X)

Figure 20. Scanning electron photomicrographs of crystallized frit HF-52-PX

HF-53-PX (1000X)

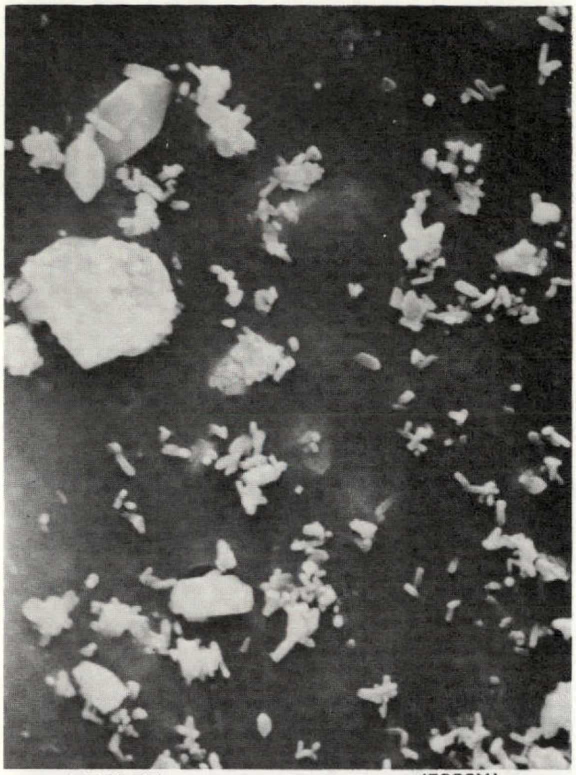

HF-53-PX (5000X)

HF-53-PX (10,000X)

Figure 21. Scanning electron photomicrographs of crystallized frit HF-53-PX

the photomicrographs depends on nucleation and growth conditions. Zircon may appear as square prisms, sometimes pyramidal, and in irregular forms and grains. Zirconia may appear in flattened, short-long prisms (compare Figure 20 with Figure 21). Again depending on growth conditions and frit composition, individual crystallities of either zircon or zirconia may grow as a dendrite (Figure 18), appear acicular (needle-like, Figures 15, 19, and 20), or display an irregular form such as the rosette shape of a portion of the zircon in Figure 10. The low thermal expansion phase β-spodumene and the α-cristabalite phase are considered undesirable. SEM studies of glasses containing either species as a major component were not carried out, thus making identification easier.

In the SEM photomicrographs, etchant pits are shallow and of irregular shape and may be differentiated thus from gas pockets (bubbles) which are relatively deep and appear spherical.

#### 3.1.2.4 Crystallization Results

The results of frit pre-crystallization prior to preparation of the enamel slip should be viewed in terms of the basic objectives, which were as follows:

1. Crystallization of the selected species zirconia and/or zircon.
2. Crystallite size controlled in the sub-micron range. Sizes preferably distributed around a mean of 0.3-0.5 micron.
3. Crystallite shape or habit preferably isotropic.
4. Crystallites distributed uniformly in the host glass.
5. Host glass content (>65-70 percent by weight) and composition controlled to provide acceptable fusion and substrate adhesion of highly, zirconia pigmented enamels in the firing range 1000-1200°C.

The first four objectives are related to optimizing optical backscattering (i.e. minimizing $\alpha_S$ in the final enamel) while retaining an adherent, refractory glass matrix. The last objective proved to be the controlling one, in regards to the finished enamel, and the hardest to achieve.

Crystallization results are summarized as follows:

1. Exclusive zircon and/or zirconia crystallization was dependent on crystal growth temperature primarily. In this regard, 900°C proved satisfactory for a range of zirconium frits (5-18 mole percent, 9-33 weight percent zirconia). Preferential zircon crystallization occurred at silica contents >~ 30 mole percent; below 30 mole percent silica, zirconia crystallized exclusively. In Tables 1, 2, 3, and 5, compare HF-53 (Figure 21) with frits HF-25, HF-28 (Figure 17), HF-20 (Figure 8), HF-10, HF-45 (Figure 19), and HF-52 (Figure 20). The latter are listed in increasing order of zirconium ion content.

2. Crystallite size was dependent primarily on nucleation effectiveness and crystal growth time. Uniform nucleation of large frit grains (0.3-1.0 cm) was observed only with frit HF-39-1, a glass containing 5 mole percent $MgF_2$ as a nucleating agent as suggested by Professor John D. McKenzie[12]. In contrast, uniform nucleation was observed in small frit grains (1-40 microns estimated) regardless of type and content of nucleating agent. This latter may be termed "surface nucleation" in contrast to "bulk nucleation" for the former. Surface nucleation may be related to surface defects or hydroxyl ion and was found to be very effective. It was conveniently achieved by wet milling of -14 mesh raw frit for 8 hours followed by oven drying of the slurry. Upon short term heat treatment, submicron crystallite size was attained (see Figures 12, 17, 19, 20, 21). Frit HF-45-1 (Figure 19) was actually oversize prior to heat treatment with resultant oversize crystallization. It is grouped here because of otherwise similarity. The effectiveness of decreasing frit grain size (from an order of 1000 to 20 microns) in producing uniform nucleation and crystallization in a given frit (HF-24) is displayed in SEM photomicrographs Figures 9-12. Note that crystallization is segregated at distorted grain boundaries in Figure 10 (500X magnification). Reduced frequency of such segregation is noted in Figure 11 (500X magnifigation). In Figure 12 (1000X magnification) such segregation has been eliminated, the result of heat treating 1-40 micron size frit. Similar results are displayed by HF-28 in Figures 16 and 17.

3. In these frits where zircon/zirconia are the encouraged crystallites, with increasing zirconium ion content in the host glass there is an increasing tendency for acicular (needle-like) growth rather than a more isotropic prismatic growth. In this regard compare in sequence: Figures 12 and 17 (7 mole percent zirconia), Figure 4 (8.5 mole percent zirconia), Figure 19 (12 mole percent zirconia), Figure 20

(15.2 mole percent zirconia), and Figure 21 (18 mole percent zirconia).

3. Uniformity of crystallite distribution is dependent on nucleation effectiveness and crystal habit. Achievement of prompt uniform nucleation at a temperature (500-550°C) well below preferred crystal growth (say 900°C) was discussed above. Crystallite appearance (habit) as prisms is preferred over needles (acicular growth). In this regard, compare Figures 12, 17, and 21 with 19, 20, and 15. Crystallite growth as dendrites (Figures 18 and 13) or other irregular forms is not desirable for reason of reduced optical backscatter potential.

4. The residual glass content and composition conducive to good pre-crystallization and later enameling with the frit remains a somewhat elusive objective. A 65-70 percent by weight residual glass content seems to be a desirable lower limit, regardless of contained flux composition. As zircon/zirconia crystallizes out, the flux-$B_2O_3$ levels increase. Establishing appropriate flux-$B_2O_3$ levels appears important for crystallization and critical for good enameling (see Section 3.1.1).

### 3.1.3 Preparation of Zirconia Pigment

Zirconium oxide (zirconia) stabilized in the cubic crystal form was selected as the pigment of main interest. Stabilized with yttrium oxide it offers a combination of desirable properties as follows:

- Good opacifier, with index of refraction 2.2
- Refractory pigment, with yttria providing high temperature stability of cubic form
- Linear thermal expansion of cubic phase desirably high, $\alpha_T \approx 100\text{-}110 \times 10^{-7}/^{\circ}C$ over the range of interest ($\sim$650 to 20°C)

Yttria-stabilized zirconia was processed by wet-milling in a vibro-energy mill (Sweco No. M18, 2.6 gal. working capacity) using 1/2 in. diam. zirconia grinding media. The grinding liquid was water. To this were added sodium hexametaphosphate ($\sim$1.0 percent by weight of liquor) and gum arabic ($\sim$0.06 percent by weight of zirconia) in order to minimize a serious problem of particulate aggregation. The pH of the mill liquor was adjusted to 7.5 - 8.0 prior to milling.

Controlled gravity sedimentation of the diluted mill liquor was used to recover a size range of approximately 0.5 - 0.7 μm in the underflow.

Subsequent re-dilution and re-sedimentation was used to reduce the sodium hexametaphosphate content. The recovered rich liquor, containing the desired solids fraction, was finally air-dried by standing in covered trays at $\sim 20^{\circ}C$. As prepared, the pigment solids contained on a weight basis:

| | |
|---|---|
| 71.94 | percent zirconia (by difference) |
| 27.8 | percent water |
| 0.2 | percent sodium hexametaphosphate |
| 0.06 | percent gum arabic |
| 100.00 | percent Total |

This pigment was produced by Tizon Chemical Corporation. Milling and sizing procedures were worked out jointly by Dr. G. H. McIntyre of Tizon and the authors. The size range has been verified in the accompanying SEM photomicrographs Figure 22 as 0.1 - 1.0 micron, averaging an order of 0.5 - 0.7 micron. Some aggregation prevails which is associated with the moisture and gum content. Upon dispersion in a slip (via milling) it is presumed that most of this aggregation is destroyed by adsorbed sodium hexametaphosphate and gum.

### 3.1.4 Slip Formulation

Having considered separately the development of a frit and a pigment, the next step is the preparation of a slurry containing both solids intimately dispersed in a liquid medium, such as water. This stable, finely divided suspension is termed a slip and enables a degree of close-packed solids deposition on a given substrate. In order to encourage a defect-free enamel from a refractory frit-refractory (high specific surface) pigment pair, one would seek a highly condensed particulate system (minimum voids) as applied. Such a dense array would minimize volumetric changes on firing and many resultant defects. Practical requirements, e.g. mill batch pigment dispersion (especially important in this opacification problem), uniform solids mixing, intimate contact with a substrate wetting/adhesion), etc. generally require use of a liquid medium (carrier) whose subsequent volatization opposes maximum solids densification.

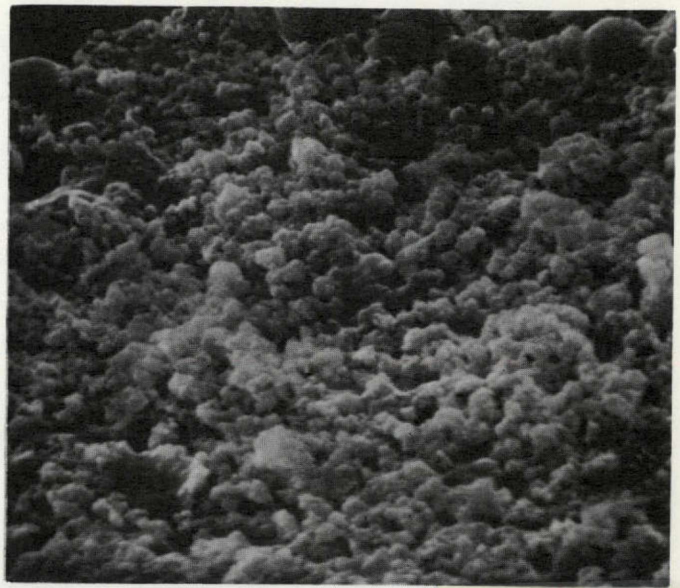

5000X

0 1 μm

This page is reproduced at the back of the report by a different reproduction method to provide better detail.

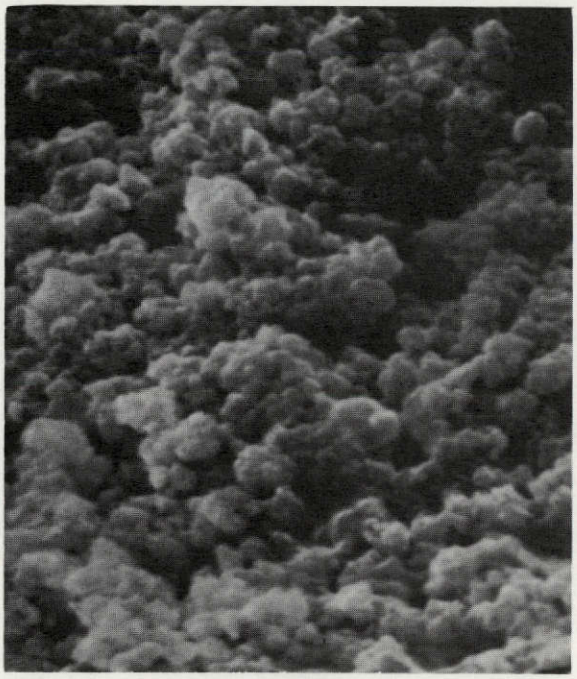

10,000X

0 1 μm

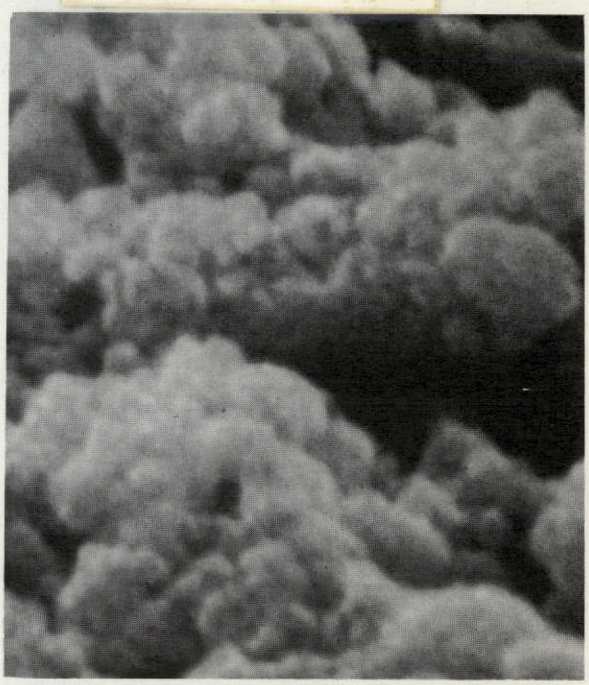

30,000X

0 1 μm

Figure 22. Scanning electron photomicrographs of yttria-stabilized zirconia pigment fraction averaging 0.5-0.7 micron in size

Solids application by dipping limits this problem, but it is considered that spray application may be the more practical for this program involving coating of one side only of large thin panels. Use of a contour-following roller was also considered as an application technique but not tried.

Formulation of a sprayable slip by ball milling typically includes consideration of certain mill additives, e.g., deflocculants, solids suspension agents, bisque tougheners etc., as well as the all important water content. Slip consistency (gel) and specific gravity are used as control parameters to guide such formulation efforts. The objective is to optimize spray deposition and so promote improved enameling. Unfortunately it has been found that idealized spraying does not guarantee good enameling.

For example those mill additions that impart bubble structure to the enamel should be avoided. These include clays and organic dispersing agents. The colloidal zirconia pigment has proven satisfactory as a suspending agent for the frit, thus eliminating the conventional use of clay. An inorganic dispersing agent, sodium hexametaphosphate, is effective for reducing aggregation of the pigment. Additions of up to 2 parts/100 parts pigment by weight appear beneficial without affecting enamel quality.

Supplemental mill-added fluxes such as LiF should be avoided because they are capable of dissolving and diffusing substrate oxides to the extent of seriously reducing opacity in ≤ 0.010 cm (0.004 in.) coatings.

Water content is somewhat variable with spray equipment and pigmentation. A suitable general guide is to adjust water content to give a slip specific gravity of 1.60-1.70. On this basis water additions of 60-70 parts/100 parts frit by weight have been typical.

The comparative effectiveness of frit presizing with mixing vs combined milling of all components has not been studied in detail. Suffice to say, 2 hour milling with a -14 mesh frit feed seems satisfactory. Improvements in this area translatable into an improved enamel seem feasible.

Summarizing, a typical slip formulation (as for HFE-45A-PX, HFE-52A-PX, HFE-53D-PX etc.) contains the following:

| Parts weight | |
|---|---|
| 100 | Frit (-14 mesh) |
| 40 | Submicron zirconia pigment (0.5-0.7 micron average size) |

Parts weight

| | |
|---|---|
| 20 | Coarse zircon pigment (-200 mesh) |
| 0.5 | Sodium hexametaphosphate $(NaPO_3)_6$ |
| 70 | Water |

For the size fraction shown, zirconia mill pigmentation above this concentration results in unacceptable enamel defects (primarily hairline tearing). Use of a coarse zircon fraction seems to reduce this tendency, especially in view of the probability that the frit is currently being overmilled.

3.1.5 Slip Application

As might be suspected, slip optimization (i.e. adjustment of rheological properties) for spray application is at best a qualitative effort. Viscosity, yield value, pH, and specific gravity measurements are helpful as controls, however. In addition to slip optimization, spray gun selection/adjustment and spraying technique constitute two major parameters important to optimum deposition of enamel solids. The substrate condition (physical and chemical nature of surface, temperature, size with respect to slip deposition rate etc.) is a final broad parameter.

Spray technique is at best a professional skill. However for purposes of reproducibility in small specimens, an attempt was made to adhere to the following conditions:

- Clean, dry argon at 35-50 psig is used as the atomizing gas.
- Apply a wet, uniform, continuous, slip film by adjusting air and slip rate, gun-to-substrate distance, and traverse rate.
- When the continuous water layer in the initial film disappears (via air- or hot plate-drying), build up the coating to final thickness without wetting. We term this "dry build-up." Alternatively, re-application on a layer which still appears wet is termed "wet build-up." Bisques (dry coatings) which result from a "wet build-up" are smoother and yield fired enamels with a smoother surface which seem less defect prone. Excessive wet build-up results in serious tearing defects.
- Double enamelling, in contrast to single enamelling above, proved to be the most effective for large panels. This involves a single spray application of a single wet layer, dried at 538°C for 1800 sec (30 min.) and fired at ~50°C below the ultimate firing temperature. This ground coat is followed by a cover coat applied in the same manner and fired at the final firing temperature.

- Dry the bisque, slowly if possible. Air drying for one half hour at 525-550$^{\circ}$C is satisfactory in most cases. Inadequate drying results in pinholes in the fired enamel.
- HastelloyX in thickness of 0.081-0.089 cm is used to typify superalloy substrates. Specimens (1 x 2 cm to 10 x 10 cm) are prepared by sandblasting (50-100 micron) and detergent cleaning.

### 3.1.6 Firing to Form the Porcelain Enamel

The ability to air-fire the dried coating (containing crystallized glass and submicron zirconia pigment) to a defect-free enamel is mainly determined by material considerations as follows:

- Mill-added pigment content and specific surface ($m^2/g$)
- Content and properties of residual glass in frit
- Minimizing outgassing during enameling

The first two factors are displayed in acceptable combination when there is sufficient glass phase of sufficient high temperature mobility and wetting ability to encapsulate both added and in-situ colloidal solid phases without defects. An unacceptable combination of these properties typically is displayed by hairline tearing in the fired enamel. Increased refractoriness of crystallized (vs uncrystallized) frits, reduced bisque strength with increasing submicron, mill-pigmentation, as well as the need for higher enameling temperatures all couple together to exaggerate the tendency for bisque cracking. That the resultant enamel tearing is related to serious expansion mismatch between bisque and metal substrate is evidenced by (a) increased enamel tearing with fired thickness and (b) increased bisque/substrate separation with increased bisque dimensions. Even with subsequent healing, the resultant hairline defect seriously degrades opacity.

The third factor relates to outgassing during enameling, i.e. in the range 1000-1200$^{\circ}$C. Its importance cannot be over-stressed especially with regard to thin coatings. Failure to eliminate this problem results in defects which seriously degrade enamel integrity and opacity both initially and after high temperature cycling. Thus outgassing during initial enameling prevents smoothing and coalescence of the surface plus excessive bubble structure in the body of the coating. The result is a major reduction in opacity and mechanical integrity. Continued outgassing can and does occur when the enamel is subjected to thermal cycling (to service temperatures of the order of 900-1000°C) and results in continued degradation of properties. Factors which contribute to this problem are listed in suspected order of decreasing importance as follows:

- Relatively volatile frit component, e.g. $B_2O_3$. (Compare HFE-54A-PX with HFE-45A-PX)
- Residual trapped gases which remain because of incomplete fining of frit
- Volatilization of chemically bound water in frit
- Combustion of gum used in pigment preparation
- Interaction of "active" frit with metal substrate at enameling temperature (1000-1200°C)
- High temperature outgassing of substrate

Whatever the causes, enamel outgassing should be minimized. The following steps are suggested to promote this:

- Avoid or minimize the use of solids which are relatively volatile at enameling temperature, e.g. $B_2O_3$
- Fine the glass melt long enough to eliminate outgassing. Resmelt after grinding if necessary
- Avoid organic or other slip additives which generate gas during enameling
- Dry the bisque at a temperature high enough (say 550°C) to promote release of chemically bound water but low enough to prevent premature bisque cracking
- Clean substrate properly

A simple frit quality control suggests itself as follows. A small portion of crystallized frit mass (unground) is placed in a transparent, fused quartz thimble. This is placed in a furnace at 1200°C and held for 600-900 sec (10-15 min.). This specimen is then quenched in air. The solid melt is then fractured and examined for bubble structure. Acceptance for enameling is based on the absence of bubble structure as compared to a control sample.

Summarizing, satisfactory firing conditions are determined by frit composition and degree of crystallization, the relative reproducibility of frit smelting, and the relative proportions of crystallized frit and mill-added pigment. For representative enamels (Section 3. 1. 4) fired on small specimens ( ≤ 10 cm x 10 cm x 0. 089 cm) of HastelloyX in air in a Kanthal-heated electric furnace, the following conditions are representative:

| Enamel | Coat | Temperature, °C | Time, sec |
|---|---|---|---|
| HFE-45A-PX or HFE-45A-PXF* | Ground | 1000 | 30-45 |
| | Cover | 1000 or 1050 | 45<br>30 |
| HFE-52A-PX | --- | ~1100 | 30-45 |
| HFE-53D-PX | --- | ~1000 | 45 |
| HF-54A-PX | Ground | 1000 | 45-60 |
| | Cover | 1100 or 1150 | 45<br>30 |

*Frit and a portion of pigment mixed well and crystallized as a mixture in an effort to reduce fusion shrinkage during enameling.

Underfiring prevents sealing of hairline tearing with opacity reduction and can cause spalling (flaking off) of the enamel. Overfiring encourages pinholes, blisters, loss of gloss, and reduced adhesion to the substrate and reduced opacity due to pinholes and blisters.

### 3.1.7 Properties of Fired Enamels

#### 3.1.7.1 Optical

Opacification efforts cannot be carried out independent of attendant effects on enamelling characteristics. This fact was encountered numerous times. The pigmentation versus frit crystallite content compromise for best opacification was made on the basis of a dual consideration of opacification and enamelling quality. This compromise is approximated by 25 percent by weight pigment and 25 percent by weight frit crystallites, yielding an order of 27 percent by volume optical backscatterers. This is an increase of ~50 percent in backscatterers over that attained in the first year's work. However, a 50 percent improvement in opacity was not demonstrated, a result believed related to the following factors:

- Increased flux composition of frits required to offset increased bisque crazing at higher enamelling temperatures. Excess fluxing yields a transparentizing bubble structure as well as providing a diffusion medium for colored interfacial oxides. This latter is especially noticeable when pigmentation is reduced (i.e., in order to improve gloss and other enamel properties).
- Inadequate, near-IR backscatter effectiveness of pigment/frit crystallite opacifier combination.

Improved definition of the flux composition in the parent frit is required and should be accomplished by modest effort. Such improvement should markedly improve opacity (as well as resistance to thermal cycling) without serious reduction in thermal expansion match with the substrate.

In regard to improved backscatter of near-IR wavelengths, broader size distribution of pigment and crystallites seems desirable. A general size range of 0.1 - 1.0 micron, centered about 0.6 - 0.7 micron should encourage scattering of 1 - 2.8 micron wavelengths. Improved pigment dispersion in the slip would also be very beneficial at all wavelengths.

Translation of controlled particulate effects into enamel opacity is displayed in Figure 23. The target of $\alpha_S \approx 0.2$ at an enamel thickness $\leq 0.01$ cm (0.004 in.) was not achieved. However, it is believed that early achievement of the above discussed remedies is feasible and will yield this goal.

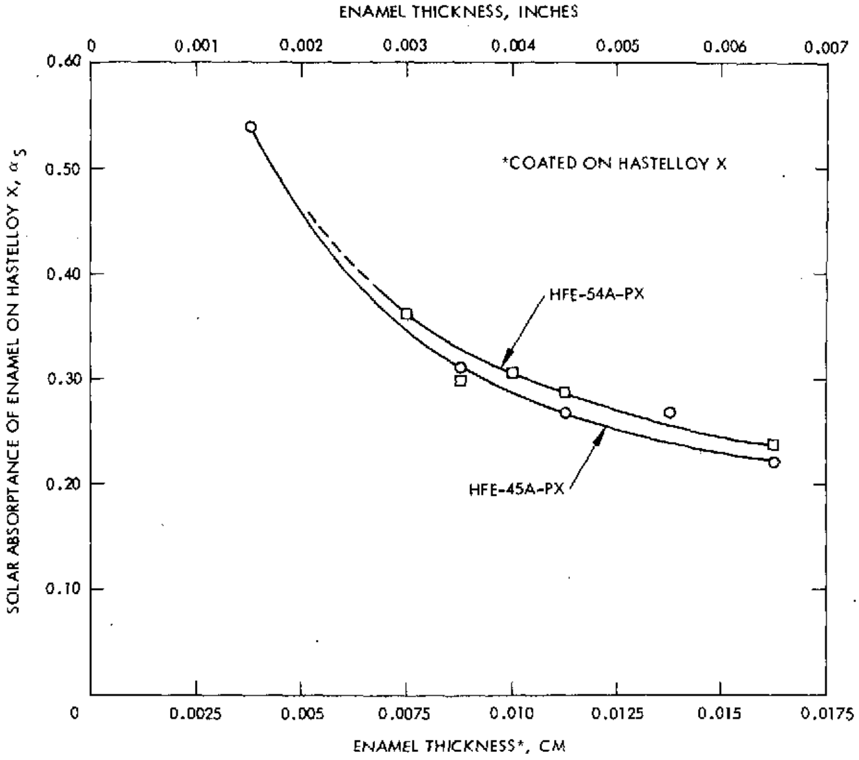


Figure 23. Effect of zirconia enamel thickness on initial solar absorptance

### 3.1.7.2 Cleanability

Despite high pigment loading with high specific area pigments, enamels with glossy surfaces have been made. For cleaning purposes, this represents an improvement over the mat finish attained in the first year's effort. As with the earlier work, discoloration from ambient sources is readily removed without affecting solar absorptance values.

### 3.1.7.3 Coating Adherence

These zirconia enamels all appear to wet the substrate (typified by Hastelloy X) well in air. Enamel linear thermal expansion values are estimated[14] as an order of $140 \times 10^{-7}/^{o}C$ over the range 20 - 650°C, representing a reasonable match with the value of $159 \times 10^{-7}/^{o}C$ estimated for Hastelloy X over this range. Bend-to-failure examination as well as thermal shock tests (see 3.1.7.4) all indicate acceptable adhesion with superalloys.

3.1.7.4 UV and Thermal Degradation of Optical and Mechanical Properties

Enamel discoloration as a result of vacuum UV irradiation with a xenon lamp is displayed in Figures 24, 25 and 26. These depict UV-induced decreases in spectral reflectance of varying thicknesses (0.0089 - 0.0165 cm) of enamel HFE-45A-PX. Practically all of this change occurs in the near-UV/visible spectral region. The change is somewhate discrete, appearing to include strong, broad absorption bands centered near 0.4 and 0.48 micron as well as weaker bands centered near 0.65 and 0.82 micron. The magnitude of these optical absorptions scales with enamel thickness and so appears independent of substrate. It is probable that these color centers involve impurity defects, the most likely being the transition metal ions.

The net effect of such radiative discoloration, in terms of a passive thermal control coating, is to increase solar absorptance $\alpha_S$ values. Such values are obtained by averaging spectral data. The above figures indicate typical $\Delta\alpha_S$ values of 0.03 - 0.04 after 983 equivalent solar hours (ESH) of

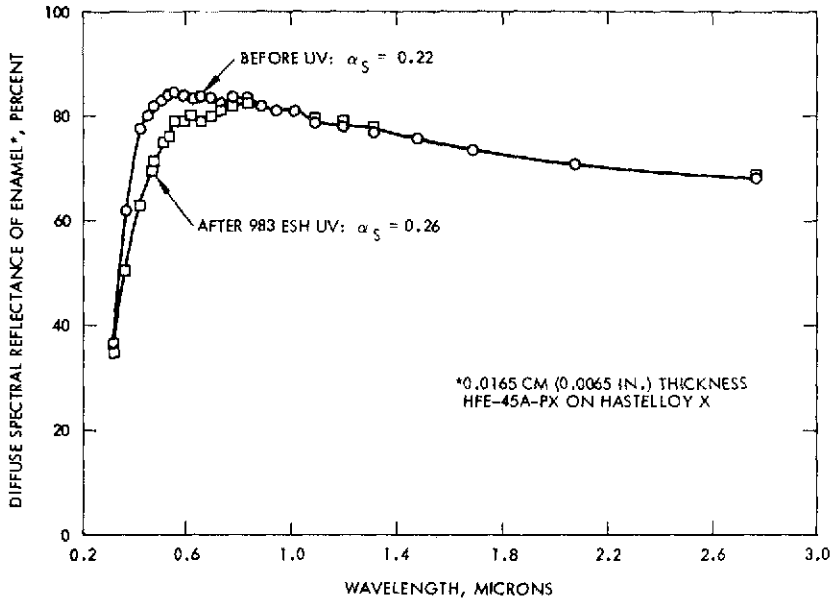


Figure 24. Change in spectral reflectance of a 0.0165 cm thickness of zirconia enamel caused by vacuum UV irradiation

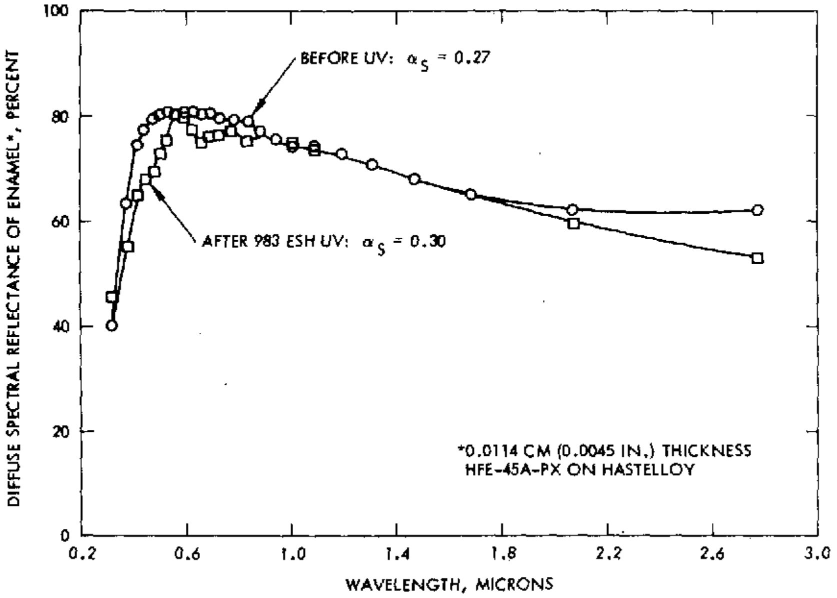


Figure 25. Change in spectral reflectance of a 0.0114 cm thickness of zirconia enamel caused by vacuum UV irradiation

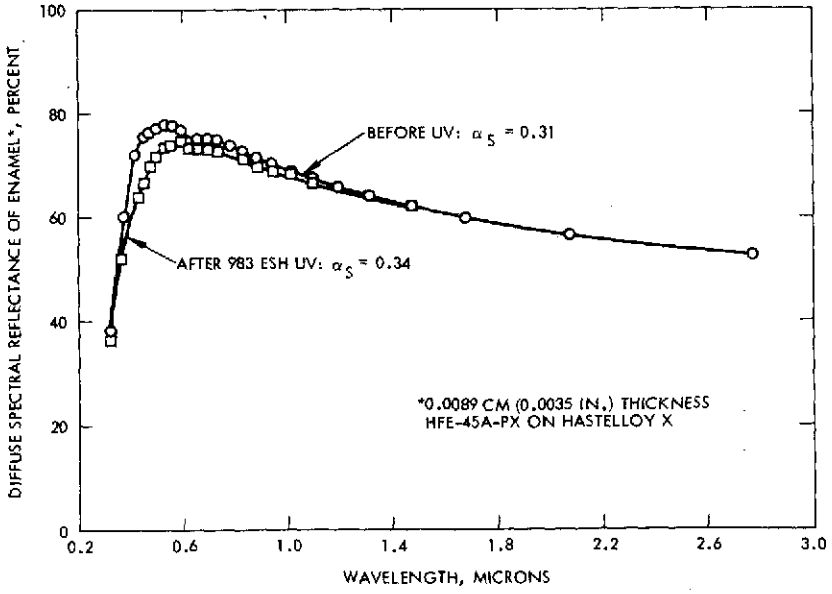


Figure 26. Change in spectral reflectance of a 0.0089 cm thickness of zirconia enamel caused by vacuum UV irradiation

simulated solar UV irradiation. It is almost certain that these can be reduced markedly by the following steps:

- Improved purity control in materials and processing
- Reduction in fluxing capability of frits to minimize transport of interfacial oxides into enamel

Thermal cycling (and thermal shock) effects were examined by raising the temperature of small specimens from ~20°C to 900°C, soaking at 900°C for 300 sec (5 min.), cooling on an aluminum block for 300 sec, and then repeating the cycle. This alternate heating/cooling was conducted in air at rates of the order of 20 - 25°C/sec. After 20 such cycles, typical changes in spectral reflectance are presented in Figure 27 and in visible appearance in Figure 28.

In the near-UV and visible wavelength regions, broad band optical absorption has been introduced which is quite similar to that observed after UV irradiation of similar enamels at the same thickness (compare Figure 27 with Figure 24). Changes in the near-IR are quite different. Thermal cycling appears to increase the metallic nature of the coating as evidenced by

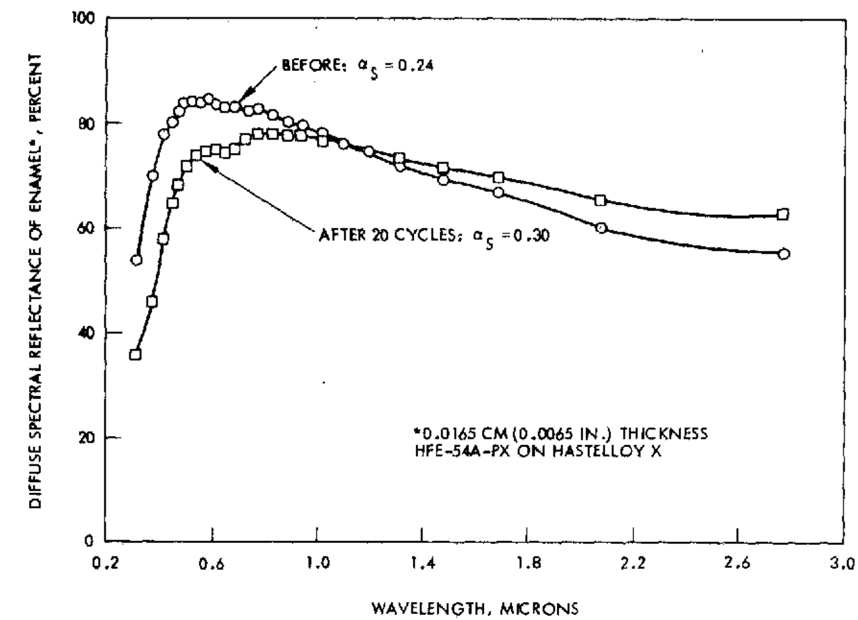


Figure 27. Change in spectral reflectance of a 0.0165 cm thickness of zirconia enamel caused by rapid thermal cycling between 20 and 900°C

ENAMEL HFE-54A-PX
(0.0165 CM COATING; 3.5X)

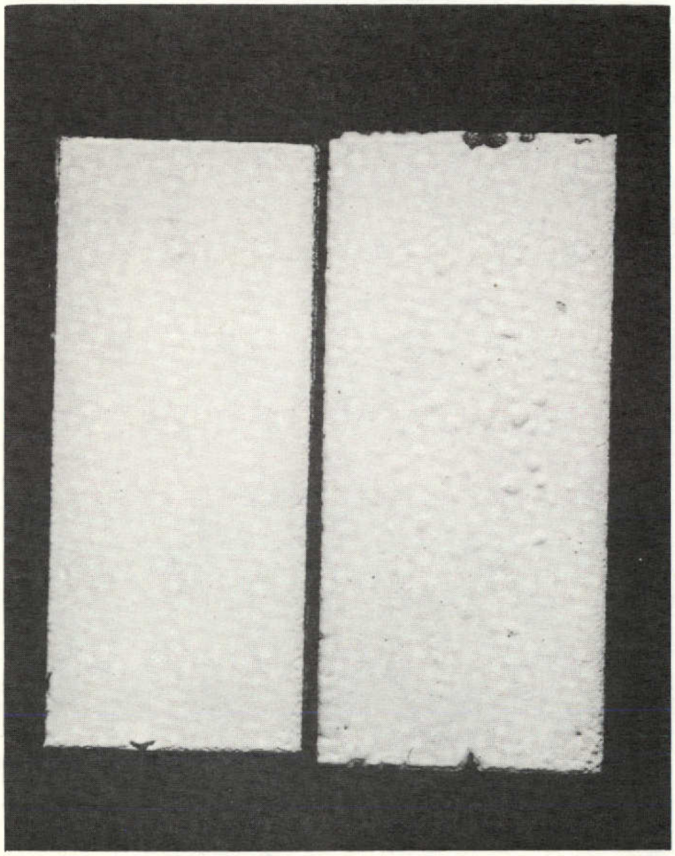

BEFORE

AFTER
20 CYCLES

0 1 CM

This page is reproduced at the back of the report by a different reproduction method to provide better detail.

Figure 28. Effect of thermal cycling on physical appearance of zirconia enamel coated on Hastelloy X

increased spectral reflectance in the region 1.2 - 2.8 microns. That this results from a transparentizing effect of excessive bubble structure in the enamel is confirmed by visual examination (Figure 28).

This enamel was fired at 1150°C. It should permit thermal cycling to 1000 - 1050°C without serious damage to opacity or mechanical integrity. Failure to allow cycling above 900°C and even then causing a $\Delta\alpha_S = 0.06$ in 20 cycles is attributed to an over-fluxed frit (see earlier discussion). This problem is believed easily remedied and should be done.

## 3.2 PROCESS SCALE-UP: HIGH TEMPERATURE ENAMELS

The objective of this scale-up investigation was to demonstrate that the porcelain enamelling process is usable on flight hardware. Scale-up efforts included the following:

| | Laboratory Size | Scale-Up Size | Scale-Up Factor |
|---|---|---|---|
| Frit preparation | 100 g | 1700 g | 17X |
| Slip preparation | 65 $cm^3$ | 260 $cm^3$ | 4X |
| Substrate coating and firing | 1 cm x 2 cm | 30 cm x 30 cm | 450X |

This work was confined to enamels HFE-45A-PX and HFE-54A-PX (see earlier discussion) spray-applied to 0.122 cm (0.049 in.) thick Hastelloy X metal. These enamels and this substrate are considered representative for demonstrating high temperature enamelling of superalloys.

### 3.2.1 Frit Preparation

The powder charge for frit smelting was prepared from requisite oxides, carbonates, or fluorides in powder form (-200 to -325 mesh). These were selected on the basis of individual impurity levels (first transition series cations, especially) ≤300 to 400 ppm. The weighed charge (2250 g) was blended about one hour by rolling (dry) in a polyethylene jar (~10,000 $cm^3$ capacity) containing Teflon mixing vanes.

Melting was carried out in a globar-heated, top-loading furnace (~15 KW maximum) of nominal 30 cm x 30 cm x 30 cm dimensions. A pressed, coarse grain, stabilized zirconia crucible (Laboratory Equipment Co. No. 728-103) was used. Inside dimensions of this straight form crucible are 9.5 cm diameter x 19.4 cm high to yield a capacity of about 1400 $cm^3$. The wall thickness is one cm. Purity is designated as 98.5 percent by weight ($ZrO_2$ > 92.2 percent, $HfO_2$ < 2 percent, CaO ≈ 4.5 percent). The furnace hearth was covered with 1 to 2 cm of alumina powder and raised to about 1550°C within 12 to 14 hours. A crucible, preheated in an auxiliary furnace to ~1200°C, was quickly transferred to the frit melting furnace and raised in temperature to 1550$^{\circ}$F. The powder was charged into the hot crucible by metal scoop through the furnace cover, about 750 g at a time. In this manner melting of the entire charge was completed within 1800 seconds (30 minutes), the liquid level being 8 to 9 cm from the top of the crucible. A platinum stirring rod with one flat blade (1.2 cm x 5 cm) was then introduced into the melt through a hole in the furnace cover. By means of an external stirring motor, the melt was stirred for about 600 seconds (10 minutes). At the end of this interval, the stirrer was removed and the melt allowed to degas for 600 to 900 seconds (10 to 15 minutes). At this point, the zirconia crucible was removed from the furnace with tongs and the glass melt was poured quickly into deionized water. A cylindrical, stainless steel water tank (33 cm ID x 63 cm high) was used, the water level being ~15 cm from the top. It was found that quenching must be carried out from the 1500$^{\circ}$C level in order to avoid premature crystallization, especially in the high zirconia frits. Thus rapid pouring is requisite to obtaining a clear (transparent) frit. A stainless pail (~10,000 cm$^3$ capacity) had been placed in the bottom of the quench tank prior to fritting. This was lifted out, and the frit was transferred to shallow Pyrex or porcelain trays for oven drying at 150$^{\circ}$C overnight.

The dry frit was next reduced to -14 mesh grains for jar milling. Crushing was accomplished by means of an alumina buckboard (plate) and muller (Coors), sizing by means of 14 mesh polypropylene screen. Typically, 200 g of this -14 mesh frit was then charged with an equal weight of water into a porcelain mill of nominal 1900 cm$^3$ capacity. The mill was loaded with ~2 kg of grinding media, 2 cm OD x 2 cm long Burundum cylinders. Jar milling of the frit was continued for $2.88 \times 10^4$ seconds (8 hours). The resultant slurry was then evaporated at 93$^{\circ}$C in porcelain or glass trays to yield a dry cake. This was crushed and blended to a free flowing powder and placed in a fireclay crucible, previously lined with a high purity, unfired alumina cake (0.2 to 0.3 cm thick).

Nucleation of this 1 to 40 micron (est.) frit grain was performed at 500$^{\circ}$C in air for 1800 seconds (30 minutes). After this, the crucible was immediately transferred to a second furnace at 900$^{\circ}$C where it was held for the same time. The crucible was then removed from the second furnace, and the fused, crystallized frit mass was immediately jarred out of the crucible directly into cold water. This quench was adequate to remove most of the adhering alumina as well as stop crystal growth.

The crystallized frit was oven dried at 150°C and then cooled. Following this it was crushed and sized to -14 mesh as described above.

### 3.2.2 Slip Preparation

A limited supply of sized, colloidal zirconia pigment prevented extensive scale-up of slip batches. This pigment shortage was associated with lack of ready availability of high purity, yttria stabilized zirconia. Scale-up was therefore confined to 200 g frit charges ground in a 1900 $cm^3$ porcelain mill with appropriate slip components (see earlier discussion of slips). A grinding period of 1.08 to 1.44 x $10^3$ seconds (3 to 4 hours) was found adequate to produce a -200 mesh slip appropriate for spray application. Overmilling is deleterious to enamelling and should be avoided.

### 3.2.3 Substrate Coating and Firing

Prior to enamelling large panels, selected optimization studies were made with a scaled-up frit batch of HF-45-PX, produced as described in section 3.2.1. Small panels, 5 cm x 5 cm x 0.088 cm, of Hastelloy X were used. Enamelling characteristics of the scaled-up frit batch were found to be significantly different from the lab size batch. In particular, the larger batch was much less refractory and displayed an unwelcome outgassing tendency which produced blisters and pinholes. Comparison of spectrographic analyses indicated a significant loss of boron, a smaller decrease in lithium, and a small increase in silicon in the lab batch, indicative of "harder" smelting and some contamination by the fireclay crucible used. To verify this, HF-54-PX was produced, and its enamelling characteristics (HFE-54A-PX) were examined. Defects associated with outgassing were largely eliminated, and the enamel was more refractory. The effect of excess $B_2O_3$ on enamelling properties (and thus indirectly on opacity) was thus revealed. It is probable that many of the other experimental frits (Tables 1, 2, and 3) contain excess $B_2O_3$ and perhaps other fluxes in excess also. A molar ratio $B_2O_3/ZrO_2 \leq 0.5$ seems reasonable. However, more precise definition of the $B_2O_3$ and other flux contents seems desirable, especially for the most promising frits, e.g., HF-45, -52, -53, and -54.

The Hastelloy X panels (30 cm x 30 cm x 0.122 cm) were first sand blasted (both surfaces) and then detergent scrubbed, rinsed, and dried. A nichrome wire hanger was then connected at two holes (15 cm apart) near one edge of each panel.

Because of a tendency for bisque/substrate separation during high temperature drying, the coating was built up in two layers, each fired separately.

The ground (prime) coat was spray-applied by airbrush (Paasche No. AUTF) as a wet coat, drying to a bisque of 0.0064 to 0.0076 (0.0025 to 0.003 in.). After several hours of air drying, this coat was oven-dried at 538°C (1000°F) for 1800 seconds (30 minutes).

These panels were fired in a 20 KW; globar-heated furnace of approximate dimensions 34 cm wide x 37 cm high x 48 cm deep (13-1/2 in. W x 14-1/2 in. H x 19 in. D). During firing, the panel was suspended by its hanger from an alumina fixture (previously located in the furnace) so that the coating faced the globar elements in one sidewall and the substrate those in the opposite sidewall. The ground coat was fired 60 to 90 seconds at 1000 to 1050°C, depending on enamel. Warpage of the order of 0.2 to 0.4 cm was observed in the 30 cm dimension.

The cover coat was sprayed on the enamelled ground coat at similar thickness and oven-dried as before. Depending on the enamel, this coat was fired 60 to 90 seconds at 1050 to 1150°C.

## 4.0 LOW TEMPERATURE ENAMELS

A preliminary study was undertaken to enamel aluminum alloys. It is recognized that aluminum is reactive with the enamel during firing and subsequent cycling to service temperatures. As a consequence, substrate preparation is an important consideration. For purposes of these frit screening tests, however, this factor was not included. Specimens of type 6061 aluminum were merely abrasive-cleaned prior to applying slip.

Aluminum enameling must be carried out at temperatures below 550-575°C. With few exceptions, even the low melting glasses are too refractory for direct enameling. Hence fluxes added as mill additions are resorted to. Typically these include KOH, $H_3B0_3$, and alkali silicates (for example Ferro #Al-30, which is a water solution).

Frit compositions range from lead-free (e.g., Ferro #Al-8) at one extreme to very high lead content (e.g., Ferro #Al-2) at the other extreme. The toxicity of lead products indicates a preference for the lead-free types, e.g., barium- or phosphate-based. Typical of pigmented enamel slips prepared from these frits are LFE-3 and LFE-4, formulated as follows:

| | Weight in Grams | |
|---|---|---|
| | LFE-3 | LFE-4 |
| Frit Al-2 | --- | 100 |
| Frit Al-8 | 100 | --- |
| Al-30 Flux | 14 | 14 |
| Rutile | 14 | 14 |
| Water | 80 | 80 |

Although optimum slip and firing conditions were not developed, initial enameling tests appear encouraging. Enameled specimens are shown in

Figure 29. The lead-free specimen (LFE-3) is over-fired with resultant pinholing. However, fusion and opacity were encouraging. The crawling observed can be remedied by improved slip formulation (e.g., including better control of fines content).

The leaded specimen (in the middle) was over-fired with resultant yellowing and loss of gloss. Improved gloss and opacity was achieved by firing at reduced temperature for a longer time (LFE-4 at right). Tearing is remediable as with crawling in LFE-3.

Small quantities of several experimental frits were prepared. These included barium-type, barium-lead types, and leaded types. Unfortunately time did not permit evaluation. However, indications are that lead-free enameling frits suitable for high opacity aluminum enamels are feasible.

This page is reproduced at the back of the report by a different reproduction method to provide better detail.

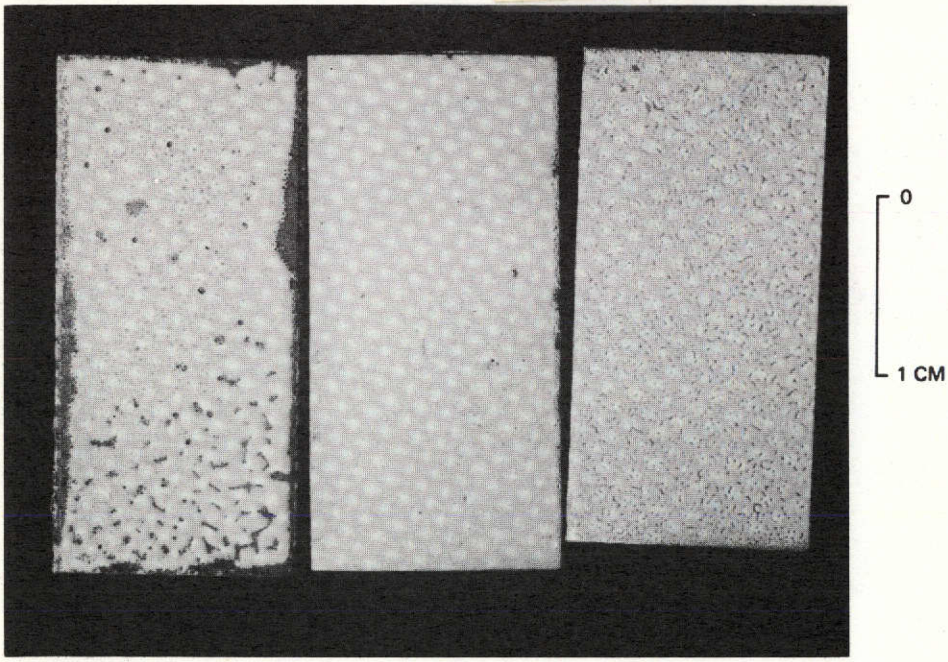


| | LFE-3 | LFE-4 | LFE-4 |
|---|---|---|---|
| FIRING TEMP, °C | 566 | 566 | 540 |
| FIRING TIME, SEC | 1200 | 1200 | 3600 |

Figure 29. Preliminary low temperature enamels fired on Type 6061 aluminum

Preceding page blank

## 5.0 REFERENCES


1. Levin, H., Auker, B.H., Gardos, M., and Blair, P.M. Jr., "Development of Porcelain Enamel Passive Thermal Control Coatings," Summary Report, NASA Contract NAS 8-27439, George C. Marshal Space Flight Center, pp. 30-31 (May 1972)

2. Huppert, P.A., "Lithia in Porcelain Enamels," Ceramic Bulletin 38(2), 59 (1959)

3. Andrews, A.I., Porcelain Enamels, 2nd Ed., The Garrard Press, Champaign, Ill., p. 53 (1961)

4. Vargin, V.V., and Kheifets, V.S., "Processes of Crystallization in Zircon Glasses and Enamels," Glass and Ceramics 22(2), 92-4 (1965)

5. Azarov, K.P., and Leskov, A.L., "Effect of the Composition of Zircon Enamels on Their Properties," Glass and Ceramics 21(7), 413-16 (1964)

6. Belyaev, G.I., and Barinov, Yu. D., "The Influence of Composition on the Whiteness and Water Resistance of Zircon Enamels," Glass and Ceramics 20(3), 142-5 (1963)

7. Jacobs, C.W.F., "Opacifying Crystalline Phases Present in Zirconium-Type Glazes," J. Am. Ceram. Soc. 37, 216-20 (1954)

8. Ibid., 258-66

9. Oel, H.J., Lachenmayr, H., and Dietzel, A., "Opacification of Glazes and Enamels by Zircon," Ber. deut. keram. Ges. 42, 462-7 (1965)

10. Sawai, I., "Glass Technology in Japan," Glass Technology 2(6), 246-7 (1961)

11. McMillan, P.W., and Partridge, G., "The Preparation of Ceramics by Controlled Crystallization of Glasses," Br. Cer. Soc. Proceedings No. 3, 249-50 (1964)

12. Private Communication; see also reference 13.

13. McMillan, P.W., and Partridge, G., Br. Patent 955653 (1964)

14. Levin, H., Auker, B.H., and Buettner, D.H., Hughes Aircraft Co. Rept. No. P72-375, NASA Contract NAS 8-27439, pp. 17-18 (Oct. 1972)